Topographic characteristics of the submarine Taiwan orogen

L.A. Ramsey, Niels Hovius, Dimitri Lague, C.S. Liu

Topographic characteristics of the submarine Taiwan orogen

L. A. Ramsey,[1] N. Hovius,[2] D. Lague,[3] and C.-S. Liu[4]

Received 21 March 2005; revised 15 December 2005; accepted 6 January 2006; published 18 May 2006.

[1] A complete digital elevation and bathymetry model of Taiwan provides the opportunity to characterize the topography of an emerging mountain belt. The orogen appears to form a continuous wedge of constant slope extending from the subaerial peaks to the submarine basin. We compare submarine channel systems from the east coast of Taiwan with their subaerial counterparts and document a number of fundamental similarities between the two environments. The submarine channel systems form a dendritic network with distinct hillslopes and channels. There is minimal sediment input from the subaerial landscape and sea level changes are insignificant, suggesting that the submarine topography is sculpted by offshore processes alone. We implement a range of geomorphic criteria, widely applied to subaerial digital elevation models, and explore the erosional processes responsible for sculpting the submarine and subaerial environments. The headwaters of the submarine channels have steep, straight slopes and a low slope-area scaling exponent, reminiscent of subaerial headwaters that are dominated by bedrock landslides. The main trunk streams offshore have concave-up longitudinal profiles, extensive knickpoints, and a slope-area scaling exponent similar in form to the onshore fluvial domain. We compare the driving mechanisms of the likely offshore erosional processes, primarily debris flows and turbidity currents, with subaerial fluvial incision. The results have important implications for reading the geomorphic signals of the submarine and subaerial landscapes, for understanding the links between the onshore and offshore environments, and, more widely, for focusing the future research of the submarine slope.

Citation: Ramsey, L. A., N. Hovius, D. Lague, and C.-S. Liu (2006), Topographic characteristics of the submarine Taiwan orogen, *J. Geophys. Res.*, *111*, F02009, doi:10.1029/2005JF000314.

1. Introduction

[2] Many mountain belts start below sea level and remain partly submerged throughout their existence. Topography sculpted by submarine processes is subsequently uplifted above sea level and forms a template on which subaerial relief develops. In turn, the products of subaerial erosion are transported into the submarine landscape and may drive its topographic evolution by erosion and/or deposition. The subaerial and submarine landscapes are intrinsically linked, and it is important to match advanced knowledge of subaerial erosion and landscape evolution with equivalent knowledge of submarine topography and erosion. Given the limitations on access, initial insights can be gained by applying terrain analysis techniques common in subaerial geomorphology to bathymetric data sets.

[3] The aim of this paper is to apply existing protocols of topographic analysis to both submerged and subaerial parts of an active mountain belt in order to identify the key topographic attributes of both and to deduce from them constraints on formative erosional processes. We use Taiwan as our example. Taiwan is a young collisional orogen with similar total relief above and below sea level and a good coverage of topographic and bathymetric data. We also have good constraints on onshore erosion rates and fluvial sediment supply to the submarine slope [*Dadson et al.*, 2003, 2004]. We begin with a brief discussion of the submarine slope in general and the important erosional features.

[4] Many active continental margins have partially submerged mountain belts. Common characteristics of such margins include a narrow shelf, a relatively steep continental slope with an overall gradient of 3°–4°, punctuated by structural complications, and a continental rise dominated by mass flow deposition [*O'Grady et al.*, 2000; *Pratson and Haxby*, 1996]. The overall shape of the continental slope is controlled by the nature and intensity of slope erosion and transport processes, and the maximum angle of repose of the substrate. Some continental slopes are straight; others grade exponentially toward the rise and/or recline toward the shelf edge, giving rise to a sigmoidal cross-sectional shape [*Schlager and Adams*, 2001]. Superposed on this

[1] Bullard Laboratories, Department of Earth Sciences, University of Cambridge, Cambridge, UK.
[2] Department of Earth Sciences, University of Cambridge, Cambridge, UK.
[3] UMR 6118, Géosciences Rennes, CNRS, Rennes, France.
[4] Oceanography, National Taiwan University, Taipei, Taiwan.

0148-0227/06/2005JF000314

general shape is a range of erosional and aggradational relief, including submarine rill and gully systems, canyons, and landslide scars.

[5] The relief offshore is created by a hierarchy of erosional and depositional processes, as it is on land. In both environments, the top of this hierarchy is likely to consist of a small set of processes lowering the channel thalweg, and the adjacent valley sides. In active, subaerial mountain belts, rivers and debris flows cut uplifting bedrock [e.g., *Hartshorn et al.*, 2002; *Stock and Dietrich*, 2003] and landslides limit the relief of interfluves [e.g., *Burbank et al.*, 1996; *Schmidt and Montgomery*, 1995]. The result is a ridge-and-valley landscape with straight hillslopes, and a well-connected, dendritic and concave-up channel network capable of evacuating erosion products over the long term. Offshore, landslides, debris flows, and turbidity currents are three of the most important erosional processes in sculpting the landscape. They occur at a range of spatial scales, from initiating small rill and gully systems to obliterating submarine canyons (e.g., the Albermale slide [*Driscoll et al.*, 2000]), and can be triggered by progressive sediment accumulation and undercutting, and events such as earthquakes, storms, gas disassociation or sea level changes.

[6] Offshore erosional processes have been documented and modeled in some considerable detail, with emphasis on the origin and evolution of submarine canyons [e.g., *Fulthorpe et al.*, 2000; *Hampton et al.*, 1996; *Mohrig et al.*, 1998; *Parker et al.*, 1986; *Pratson and Coakley*, 1996; *Spinelli and Field*, 2001]. Submarine canyons sculpt hundreds to thousands of meters of offshore relief and can be several tens of kilometers wide. They vary in form from straight, steep-sided, V-shaped channels to gentle, meandering U-shaped valleys and generally have concave-up long profiles. Initially, submarine canyons were thought to originate at sea level lowstands where rivers were able to deliver sediment well below the shelf break [*Daly*, 1936], and turbidity currents were thought to drive their formation [*Heezen and Ewing*, 1952; *Kuenen*, 1937]. However, the abundance of submarine canyons with steep head scarps well below the shelf break [*Twichell and Roberts*, 1982] indicates that canyon initiation by spring sapping [e.g., *Dunne*, 1980; *Orange et al.*, 1994] and propagation by retrogressive slope failure may also occur [*Farre et al.*, 1983]. *Orange et al.* [1994] highlighted the important feedback between the hydrologic and geomorphic systems. They suggested that excess pore pressures (head gradients) trigger slope failure at the head of the submarine canyon, and that it is the interaction of local fluid flow fields in neighboring submarine canyons that controls canyon spacing and hence drainage density offshore. The excess pore pressures required to cause slope failure are controlled by physical variables such as material strength, regional slope, rock permeability, and fluid discharge, and the canyon boundaries may migrate in time. Seepage induced failure is important in some subaerial environments but channelized overland flow dominates. Other processes such as sediment creep, slumping, bedrock jointing, and current action can aid the excavation of canyons and the downslope displacement of their fill [*Shepard*, 1981].

[7] Gully systems have smaller-scale relief and often converge with submarine canyons at high angles to form a dendritic pattern directly comparable to subaerial drainage networks. They are thought to grow by retrogressive slope failure but are relatively short (0.5–5 km) and narrow (<250 m wide) and have a depth of up to 40 m [*Buffington and Moore*, 1963]. Rills are sets of low-relief, subparallel, linear gullies cut purely by sediment flows [*Pratson et al.*, 1994]. They can be up to 300 m wide and 40 m deep, form on low-gradient slopes and are possibly a precursor to canyon formation [*Pratson and Coakley*, 1996].

[8] Submarine erosional features have been described in direct analogy with subaerial landforms as far back as 1976 [*Chough and Hesse*, 1976], implying close parallels in their formation and evolution despite the important differences between the densities and viscosities of air and water [*Orange et al.*, 1994; *Peakall et al.*, 2000]. A logical next step in submarine geomorphology is to gain a full quantitative understanding of the similarities and differences between submarine and subaerial topography.

[9] In the following sections, we introduce the methods used for characterization of subaerial and submarine topography. We go on to show that, although the onshore and offshore landscapes of Taiwan are superficially very different, their quantitative topographic characteristics are similar. This raises the compelling question as to whether similarities in topographic form can originate from similarities in formative erosional process, despite obvious differences in boundary conditions. Given that the current metrics for distinguishing landscapes are diagnostic, we attempt an exploratory interpretation of our results, fully aware that the subject of submarine geomorphology is in its infancy.

2. Topographic Analysis

[10] The aim of terrain analysis is to identify the key attributes of topography and spatial organization of the landscape, and to derive constraints on the mechanics of the principal erosional processes. Mountain topography can be considered on three spatial scales: the mountain belt scale, the catchment scale and the subcatchment scale. These length scales determine the type of topographic analysis undertaken and the inferences made.

[11] At the mountain belt scale, topographic analysis provides an insight into the balance between tectonic input of rock mass and erosion. For instance, along-strike variations in mean elevation can result from gradients in climatic forcing of erosion, or substrate erodibility [*Montgomery et al.*, 2001], or from gradients in rock uplift rate or lateral propagation of mountain building [*Duncan et al.*, 2003; *Willett et al.*, 2001]. Mean topographic profiles perpendicular to the main structural trend can also help determine whether the mountain belt obeys a critical wedge geometry [*Suppe*, 1981] and can provide a macroscopic measure of its mechanical properties and the interactions between tectonics and erosion [*Hilley and Strecker*, 2004; *Saffer and Bekins*, 2002; *Whipple and Meade*, 2004].

[12] At the catchment scale, the drainage network dictates the organization of the relief and the routing of sediment, and connects the landscape to the local base level. Channel profiles document the local competition between rock uplift, fluvial incision and sediment supply by the hillslopes [*Duvall et al.*, 2004; *Sklar and Dietrich*,

1998; *Snyder et al.*, 2000]. Abrupt increases in slope along channel profiles (knickpoints) can indicate localized rock uplift or insufficient fluvial cutting [*Lavé and Avouac*, 2001; *Seeber and Gornitz*, 1983; *Wobus et al.*, 2003], a simple change in lithology, or the upstream migration of perturbations originating lower in the profile [*Whipple and Tucker*, 1999]. Smooth, concave-up profiles are typical, in theory, of systems underlain by a uniformly erodible substrate in which the balance between rock uplift, channel incision and sediment transport is constant along stream [*Howard et al.*, 1994]. However, smooth, concave-up profiles are also found away from steady state, especially if channels are transport limited [*Whipple and Tucker*, 2002; *Willgoose*, 1994].

[13] At a finer scale, topographic analysis details the spatial distribution and nature of erosional processes and may yield information on their mechanics and rates. Ideally, the topographic signature of a given process should be unique. This would allow us to recognize processes operating in a submarine setting by a comparison with subaerial relief. However, we stress that this is not systematically the case. For example, different models of bedrock channel evolution (opting for the transport of sediment or the incision of bedrock as a limiting factor) predict the same channel profile at steady state (when erosion rate and profile geometry are constant with time) [*Lague and Davy*, 2003; *Whipple and Tucker*, 2002]. Yet, topographic analysis has proved a powerful tool, especially since the advent of high-resolution Digital Elevation Models (DEMs). The recognition that topographic slope and water discharge are first-order controls on erosion, has underpinned their interpretation. Upslope area can be used as a proxy for water discharge and can be estimated, along with local slope, from DEMs [*Band*, 1986; *Tarboton*, 1997]. It is common to plot these data on slope-area diagrams that can be used (1) to determine the spatial distribution of erosional processes in a drainage basin (i.e., process domains) [*Dietrich et al.*, 1993; *Ijjasz-Vasquez and Bras*, 1995; *Lague and Davy*, 2003; *Montgomery and Foufoula-Georgiou*, 1993; *Tarboton et al.*, 1989; *Tucker and Bras*, 1998], (2) to quantify the relative impact of tectonics, climate and lithology on topographic relief [*Kirby and Whipple*, 2001; *Kobor and Roering*, 2004; *Lague et al.*, 2000; *Snyder et al.*, 2000], and (3) to test the predictions of theory and experiment [*Hancock and Willgoose*, 2001; *Howard*, 1997; *Lague et al.*, 2003; *Tucker and Whipple*, 2002; *Willgoose et al.*, 1991]. In this study, we are particularly interested in the first approach: the identification of process domains.

[14] Process domains are separated by breaks in the relationship between slope and drainage area that occur at particular threshold values. A power law relationship between local slope and drainage area has been found for many river systems [*Flint*, 1974; *Hack*, 1957; *Kirby and Whipple*, 2001; *Sklar and Dietrich*, 1998; *Snyder et al.*, 2000; *Tarboton et al.*, 1989; *Tucker and Bras*, 1998]:

$$S = kA^{-\theta} \tag{1}$$

where k is the characteristic channel steepness (or steepness index), and θ is the slope-area exponent (or concavity index) with typical values between 0.3 and 0.7 (see *Tucker and Whipple* [2002] and *Whipple* [2004] for a review). This power law relationship is generally observed above a threshold drainage area of between 0.1 and 5 km^2. Below this threshold area water does not accumulate regularly in sufficiently large quantities for persistent fluvial incision, and topographic change is typically dominated by mass movements that range from landslides and rock avalanches to soil creep and debris flows. The slope-area signature of these processes is still discussed. Some authors have reported a power law with a small slope-area exponent (0.1–0.3) [*Lague and Davy*, 2003; *Montgomery and Foufoula-Georgiou*, 1993], and others a convex-up relationship [*Stock and Dietrich*, 2003]. Nevertheless, for sufficiently rapid river incision small subcatchments of a drainage basin ultimately reach the critical slope for landsliding. This critical slope is a function of rock lithology, density and connectivity of discontinuities in the rock mass, and pore pressure [*Burbank et al.*, 1996; *Schmidt and Montgomery*, 1995; *Tucker and Bras*, 1998]. Given that channels commonly occupy only a few percent of land area, catchment-wide slope statistics are dominated by the hillslopes.

[15] We also choose to measure local curvature to provide a simple measure of the degree of dissection of the landscape (the rugosity). The curvature differentiates convex areas (dominated by diffusion-like processes) and planar areas, from concave areas typical of incised topography.

3. Taiwan

[16] Taiwan is built from the rapid and oblique convergence of the Luzon Arc, riding on the Philippine Sea plate, and the Asian continental margin (Figure 1) [*Barrier and Angelier*, 1986; *Teng*, 1990; *Suppe*, 1980]. The orogen links the Ryukyu and Manila subduction systems and forms a linear, roughly north-south oriented mountain belt that levels out at peak elevations of around 4 km above sea level. South of Taiwan, the subduction of the Asian margin beneath the Philippine Sea plate forms an accretionary prism that is progressively uplifted above sea level. More recently [*Shyu et al.*, 2005] have challenged this traditional view, and they suggest that the submarine ridge south of Taiwan is in fact a continental sliver, structurally continuous with the Central Range to the north. Northeast of Taiwan, the subduction of the Philippine Sea plate beneath the Asian margin results in back-arc extension at the Okinawa Trough and extension of the Taiwan orogen. Thus Taiwan marks the interaction of the two oppositely dipping subduction systems and provides a unique opportunity to study the mountain building process through time.

[17] The central segment of the Taiwan orogen has been described by some as a doubly vergent wedge [*Willett et al.*, 1993]. It consists of a shallow, easterly dipping fold-and-thrust belt [*Davis et al.*, 1983] in Miocene-Quaternary sediments in the west, and a metamorphosed continental margin sequence [*Ernst*, 1983], rapidly exhumed [*Willett et al.*, 2003] on steep, westerly dipping faults in the east (see cross section, Figure 1). The existence and significance of a range-bounding structure in the east is a matter of debate, and other workers interpret Taiwan as a one-sided wedge with an eastward steepening basal decollement [*Carena et al.*, 2002; *Davis et al.*, 1983; *Suppe*, 1981]. Regardless, the Central Range extends along the backbone of Taiwan and is

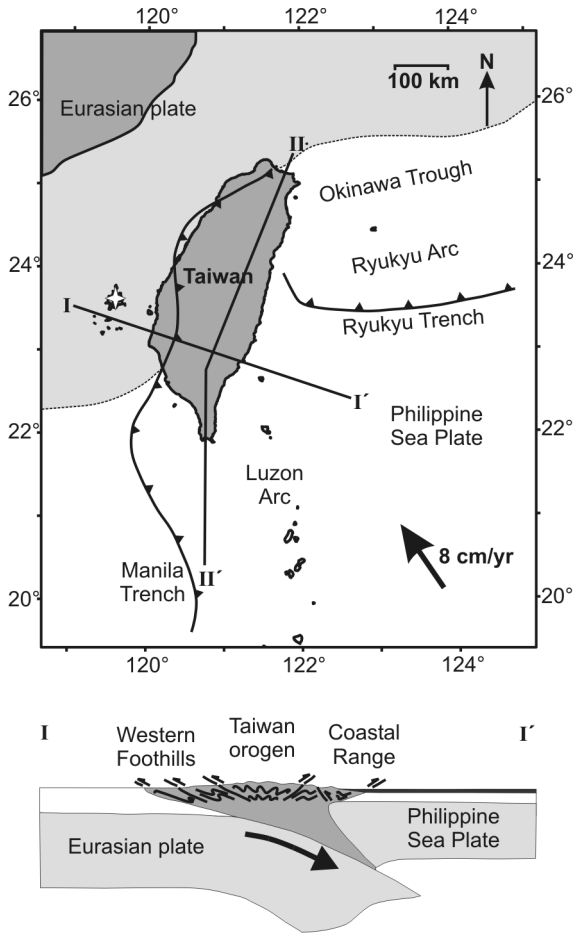

Figure 1. Tectonic setting of Taiwan: collision of the Eurasian plate and the Philippine Sea plate with a flip in the subduction polarity beneath Taiwan. The approximate extent of the Chinese continental margin is shown by the light gray area. The Philippine Sea plate is moving with a velocity of 8 cm/yr at an azimuth of 306° relative to Paisha on the Chinese continental margin (marked by a white star) [*Yu et al.*, 1997]. Line I-I′ shows a cross section of the orogen from the Western Foothills fold-and-thrust belt in the west to the accretion of the Coastal Range in the east [after *Teng et al.*, 2000]. The length profile II-II′ is shown in Figure 4.

composed of bands of sedimentary rocks increasing in metamorphic grade to the east. The smaller Coastal Range bounds the east coast of Taiwan. It consists of accreted segments of the Luzon volcanic arc, dominated by sandstone/mudstone rhythmites and volcaniclastic conglomerates. Offshore to the east, the orogen shows a further 5 km of relief and the absolute base level lies over 100 km from the coast in the Huatung basin. Offshore to the west, the orogen is flanked by a shallow marine flexural foredeep [*Lin et al.*, 2003].

[18] The subaerial eastern flank of the Central Range is drained by regularly spaced transverse rivers, cross cutting the structural grain. Steep hillslopes with thin (<1 m), discontinuous regolith and soil cover flank these rivers. Valley floors are in bedrock, mantled by discontinuous, coarse-grained lag deposits. The Coastal Range is a barrier to these transverse rivers (Figure 2). Runoff is collected along the Longitudinal Valley and diverted around the northern and southern tips of the Coastal Range in the Hualien River and Peinan River respectively. These rivers are connected with deep offshore canyons that drain far into the Huatung basin (Figure 2). The Hsiukuluan River is the only drainage to cut across the width of the Coastal Range. Offshore, the Hsiukuluan valley continues in a broad, sediment filled depression with a uniform slope of 5°. There are numerous, smaller submarine valleys along the eastern coast (Figure 2) that eventually merge into one of the three larger canyons. Most of these smaller submarine valleys are not obviously connected with subaerial drainage systems, and their formation may be due entirely to marine processes.

4. Data and Methods

[19] Digital elevation data exist for almost the entire Taiwan orogen, but the resolution is not uniform. The subaerial part of the orogen is described by a photogrammetrically derived digital elevation model (DEM) with 40 m by 40 m grid cells. Swath bathymetry data cover the submerged part of the orogen. South of Taiwan, these data are coarse and posted at 1 km resolution. Better data, collected by the R/V L'Atalante in 1996, are available for the areas east and west of Taiwan. The resolution of the Atalante swath bathymetry varies with water depth. To achieve uniformity, these data have been sampled at 100 m intervals, but higher-resolution DEMs can be constructed for shallow water depths. Owing to navigational restrictions, there are no detailed bathymetric data available for the narrow shelf area off eastern Taiwan. This data gap has been patched with interpolated spot soundings, but the shelf bathymetry remains largely unconstrained. The 40 m subaerial data set has been resampled at 100 m and merged with the marine data to pursue a complete topographic analysis of eastern Taiwan. An overview of the merged data is given in Figures 2 and 3.

[20] We have extracted a series of topographic attributes from these data at a range of length scales. We have computed topographic swath profiles across the orogen, perpendicular to its north-south structural grain using the 100 m DEM both onshore and offshore. For each 15 km swath, we have computed the minimum, mean and maximum elevation. Local relief was calculated as the difference between maximum and minimum elevation. The width of the swaths was chosen to coincide with the average width of transverse catchments in the subaerial eastern flank of the Central Range. This has eliminated location prejudice from our estimates of minimum, mean and maximum elevation. We have derived the drainage network from the DEM using a standard steepest slope flow-routing algorithm. Local slope is defined accordingly as the steepest slope calculated using the nearest pixels. We determined the drainage network for the 40 m subaerial digital elevation model and the merged 100 m resolution data set. Mindful of scaling issues [*Stark and Stark*, 2001], we have analyzed the 40 m subaerial DEM and 100 m bathymetric data primarily, but considered finer-scaled, shallow marine bathymetric data where possible (50 m by 50 m grid cells). For display purposes, we

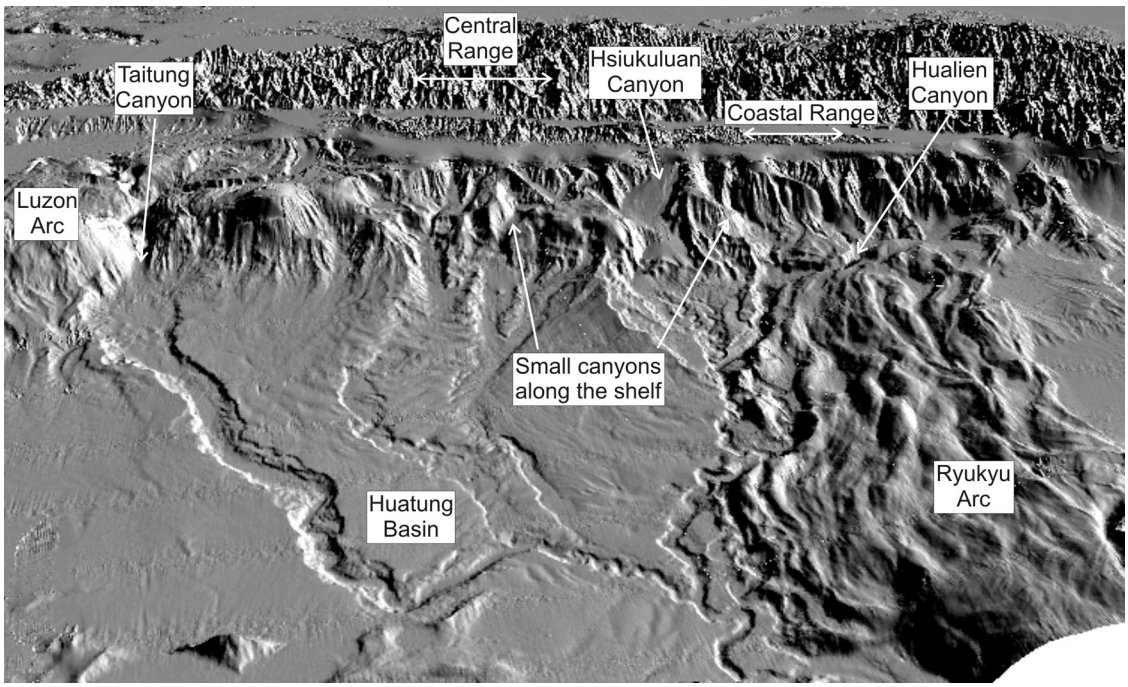

Figure 2. Perspective view of the 100 m DEM of Taiwan illuminated from the north and viewed from the east. The elevation is at three times vertical exaggeration. The Coastal Range is ~135 km long and directs the drainage from the Central Range to the Hualien and Taitung canyons. Note the large offshore canyon systems in the foreground and the erosional nature of the offshore slope.

have assumed that the upslope area required for channelization is 1 km^2 both onshore and offshore. Use of this cutoff value is supported by slope-area analysis (see section 5). Finally, local curvature was calculated by fitting a second-order polynomial surface to a moving window, the size of which can be varied to estimate curvature at a range of length scales. We define the local curvature as the maximum curvature of the topography derived from the polynomial surface.

5. Results

5.1. Regional Survey of Topographic Attributes

[21] Characterization of the topography at the mountain belt, catchment and subcatchment scale provides discriminative information about the tectonic uplift, material properties and defining erosional processes of the landscape. Prior to our detailed, catchment-scale study of submarine and subaerial topography, we review the major topographic attributes of the Taiwan orogen. Throughout, our focus is primarily on eastern Taiwan, where sediment cover is limited, and erosion is dominant both onshore and offshore (Figure 2). In contrast, the shallow marine foreland of western Taiwan contains little or no erosional topography and therefore does not meet the requirements of our study.

[22] A north-south 15 km swath profile (Figure 4) along the ridgepole of Taiwan clearly illustrates the gradual emergence, highstand, and subsequent decline of the orogen. Starting at a water depth of ~2.5 km, the height of the Taiwan orogen increases steadily from south to north, before leveling out at ~2.5 km above sea level. Several authors suggest that the constant mean elevation of central Taiwan is indicative of a sustained balance between tectonic input and erosional removal of mass [*Li*, 1976; *Suppe*, 1981] required for topographic steady state [*Willett and Brandon*, 2002]. Similarly, increasing orogen height in the south of Taiwan would suggest that the rate of tectonic input of material is outpacing the rate of erosion. Yet without quantitative constraints on the long-term erosional flux from the Taiwan orogen, it is difficult to substantiate this interpretation. The presence of a promontory on the Asian margin, and the Luzon Arc may place additional controls on the height of the Taiwan orogen.

[23] East-west swath profiles, taken from the merged 100 m data set and perpendicular to the structural grain of the orogen, show the width of the mountain belt increasing to a constant from south to north (Figure 3), mirroring the mean elevation. The east-west profiles of the mean elevation of the subaerial mountain belt capture its characteristic asymmetric wedge shape. The western and eastern flanks of the orogen are considered to be the pro-wedge and retro-wedge, respectively. While the surface taper of the pro-wedge terminates at sea level in western Taiwan, it could be said that the retro-wedge continues offshore, east of the island. This is true only if one considers that the Coastal Range is an integral part of the Taiwan orogen, rather than a rigid backstop to it. The latter is the more common interpretation, but our cross profiles suggest that the former may be more appropriate. Regardless, the taper of east Taiwan is fairly constant along strike at 5–6°, both onshore and offshore. An exception is the steeper (8°) offshore section in profile A-A′, Figure 3. The saturation and pore pressure of the crustal material may be controlling factors on the geometry

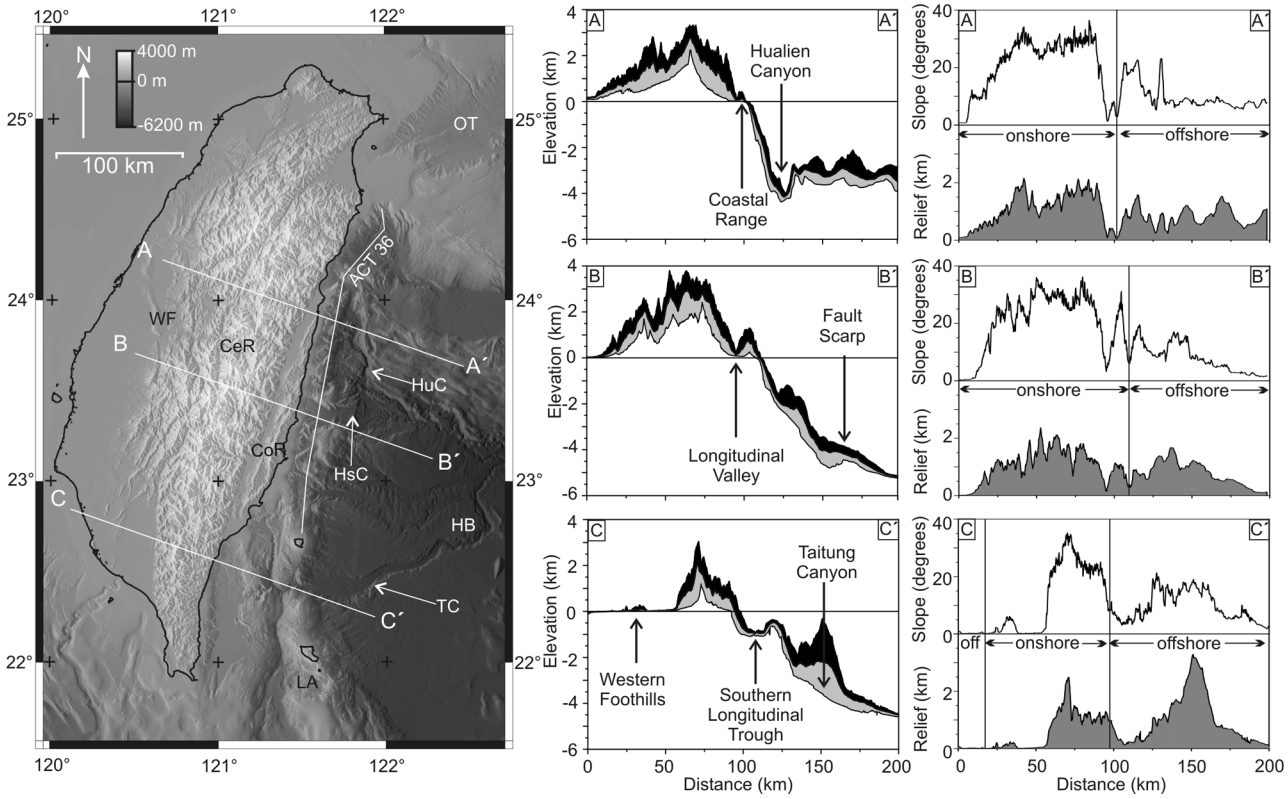

Figure 3. The 100 m resolution digital elevation model (DEM) of Taiwan and the surrounding area. The positions of swath profiles, A, B, and C, and the seismic line ACT 36 are included as thin white lines. CeR, Central Range; CoR, Coastal Range; HuC, Hualien Canyon; HsC, Hsiukuluan Canyon; LA, Luzon Arc; OT, Okinawa Trough; HB, Huatang Basin; TC, Taitung Canyon; WF, Western Foothills. Profiles A, B, and C illustrate the maximum, mean, and minimum topography and the corresponding local slope and relief taken from the 100 m DEM. Note the increasing width of the mountain belt to the north and the higher slopes onshore.

of an orogenic wedge [*Davis et al.*, 1983]; the uniform taper of east Taiwan, offshore and onshore, suggests that the wedge maintains its state of pore pressure as it is pushed above sea level [*Saffer and Bekins*, 2002]. We note that the taper of east Taiwan is similar to that of other active continental margins [*Pratson and Haxby*, 1996]. The uniformity of continental margin slopes has been attributed to pervasive slope failure [e.g., *Adams and Schlager*, 2000], turbidity currents [*Kostic et al.*, 2002], and internal waves [*Cacchione et al.*, 2002]. These explanations can be ruled out for subaerial Taiwan, and we favor the critical wedge explanation instead.

[24] Next, we consider the distribution of minimum local elevation across the orogen. Onshore, and especially east of the main divide, the minimum elevation profiles have a relatively smooth, concave-up shape that is closely related

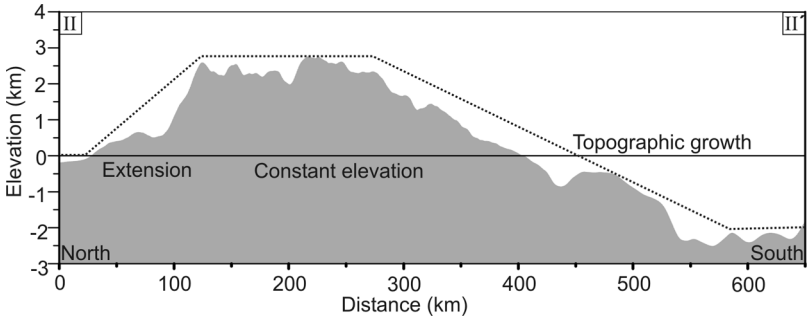

Figure 4. A 15 km swath profile along the length of Taiwan (the position of the profile is given in Figure 1). Note the steady increase in height of the orogen in the south, the constant elevation at a height of 2.5 km in the center, and the rapid collapse of the orogen to the north in association with back-arc spreading. The accretionary prism increases in elevation in the south with no appreciable segmentation between the offshore and onshore domains.

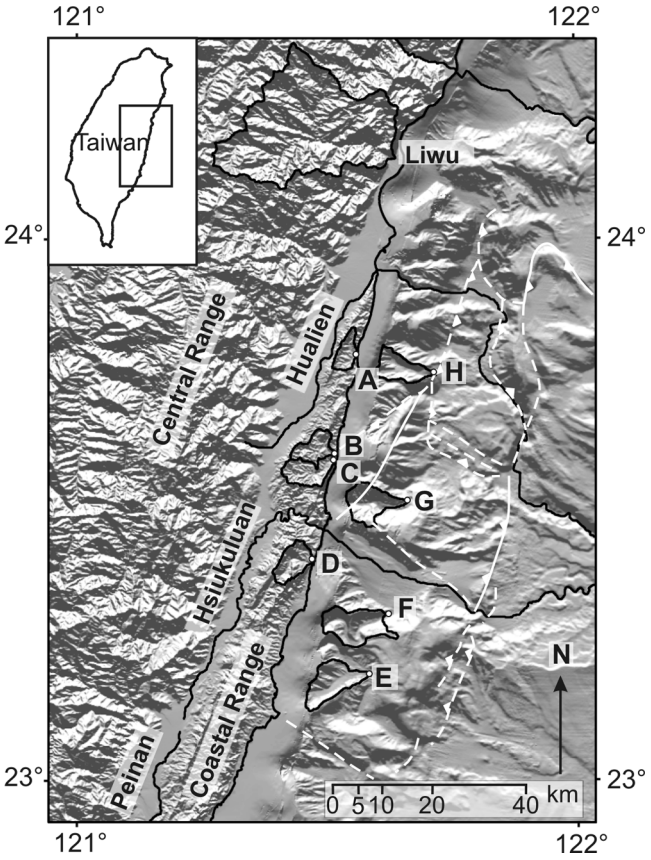

Figure 5. The 100 m DEM of the east coast of Taiwan illuminated from the northeast (position shown by the inset) and the location of the nine basins included in this study (A–H and Liwu). The extent of each catchment is shown by a solid black line, and the position of the outlet is shown by a small white dot. The Hualien and Peinan rivers are shown in black and flow around the north and south of the Coastal Range, respectively, and the Hsiukuluan River cuts across the Coastal Range. Note the poorly resolved data gap immediately offshore. Faults as mapped by *Malavieille et al.* [2002] are shown in white (thrust faults show teeth on the upper plate; minor faults have no teeth).

to the longitudinal profiles of the major rivers draining the mountain belt (Figure 3). These profiles grade to sea level and there is a sharp, convex transition to the marine domain. Below sea level, minimum elevation profiles are typically straight or slightly concave, with large (0.1–1 km) knickpoints in some sections and overall gradients of 2°–5°. A notable exception is the concave minimum profile of section C-C′ (Figure 3) which traces the smooth base of the Taitung canyon to the east of the Luzon Arc.

[25] The distribution of local relief across Taiwan (Figure 3) further highlights the contrasts in the dissection of the subaerial and submarine landscapes. Onshore, local relief is typically 1–2 km throughout Taiwan, except for the extreme south, north and west. While the subdued relief in the north and south cannot be seen in the profiles shown in Figure 3, the westward decrease of relief is clear. Assuming that hillslope angle is at a threshold and dependent on lithology only, we attribute this decrease to the weakness of the poorly consolidated, Plio-Quaternary sediments that crop out in the Western Foothills fold-and-thrust belt [*Hickman et al.*, 2002; *Hsieh and Knuepfer*, 2002]. Lithology-controlled variations in local relief may be superposed on an overall westward decrease of relief associated with the gentler taper and lower uplift rates of the pro-wedge [*Whipple and Meade*, 2004]. Further east, fluvial dissection of stronger metasediments gives rise to uniform, high local relief. Offshore east Taiwan, profiles A-A′ and B-B′ suggest the submarine local relief is consistently lower at 0.5–1.5 km and diminishes toward the abyssal plain (Figure 3), as is common along continental margins [*Pratson and Haxby*, 1996; *O'Grady et al.*, 2000]. In relief profile C-C′, the Taitung Canyon is a clear exception and descends over 4 km in only 15 km horizontal distance where it cuts across the Luzon arc. This is the greatest local relief of the whole Taiwan orogen.

[26] Mean local slopes (Figure 3) are consistently high in the subaerial mountain belt, at 30°–35°, but lower in the weaker sediments of the Western Foothills. Local slopes offshore in the (accreted) Luzon arc are 15°–20°, even though similar rocks in the Coastal Range support slopes of ~30°. From this analysis of the 100 m merged data set, we note that both local relief and local slope are more variable onshore than offshore, and the characteristic length scale of these variations is shorter on land. Taken together, these observations suggest that the degree of dissection of the topography is greater on land than offshore.

5.2. Channel Network

[27] To expand our findings, we now pursue a detailed analysis of individual river catchments and submarine channel systems and attempt to link our interpretations to formative erosional processes. Onshore, there is a close match between the drainage network extracted from the DEM and the stream network indicated on 1:10,000-scale topographic maps. Inconsistencies arise in flat, low-lying areas; regions of stream capture and dry valleys [*Deffontaines et al.*, 1994]. There is no independent material available to validate the calculated submarine channel network.

[28] In the eastern Central Range, drainage networks are dendritic with trunk streams perpendicular to the structural grain of the mountain belt. Total stream length from the headwaters to the range front is typically around 70 km, and catchment areas range upward to ~750 km^2. Lower-order streams are closely spaced, resulting in a high drainage density and a notably dissected landscape. Rivers within the Coastal Range are typically 15 km long, have a catchment area of <100 km^2 and a lower drainage density. Moreover, some Coastal Range trunk streams run parallel to the structural grain instead of across it. The water discharge and sediment load of these rivers is essentially unknown.

[29] The Hualien, Hsiukuluan and Peinan rivers collect most runoff from the eastern Central Range. They are each connected with a major submarine canyon. Elsewhere, the link between subaerial streams and submarine channels is unclear because of the nearshore data gap. Below the narrow (<10 km) Coastal Range shelf, a number of gullies and smaller canyons are present within the upper part of the submarine orogen slope (Figures 2 and 5). Canyon heads

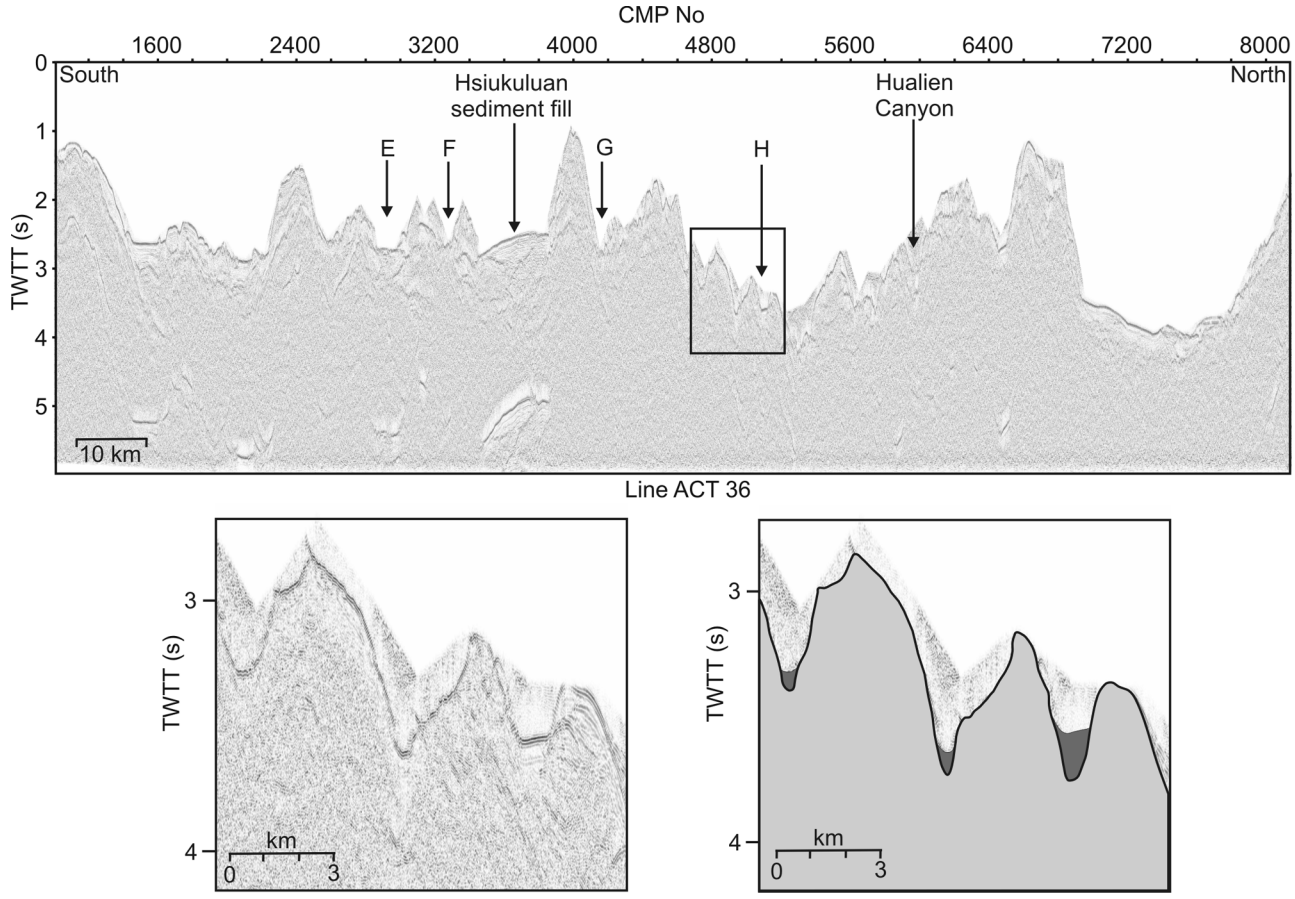

Figure 6. (top) North-south migrated six-channel profile line off the east coast of Taiwan; see Figure 3 for position. The locations of the four offshore channels, E–H, and the Hualien and Hsiukuluan canyons are included. The channels have a V-shaped cross section with some sediment fill in the base. The Hsiukuluan Canyon has a large amount of sediment fill aggrading in the channel. (bottom) Blowup of the boxed region to more clearly show the V-shaped channels and sediment fill. The right-hand image is an annotated interpretation (fill is shown in dark gray).

appear to coincide with the shelf edge, but they are poorly resolved in our data. Downslope, gullies and canyons merge to form a coarse, dendritic channel pattern. Some canyons are straight; others meander, but most run perpendicular to the general trend of the orogen. The lower part of the submarine slope is less incised. It is characterized by several large (10–30 km), convex promontories and topographic steps tracing major reverse faults [*Malavieille et al.*, 2002] (Figure 5).

[30] On the basis of lithology and system size, we have selected several channel systems for further analysis. Offshore, we have chosen four channel systems of similar size, set in the upper part of the submarine slope (Figure 5). Their channel lengths range from 14 km to 25 km, and the offshore areas contributing 'runoff' are between 60 km^2 and 100 km^2, although the channel systems are artificially delimited at the shelf edge. In the available topographic data, there are no obvious channels linking these offshore systems with onshore catchments across the shelf. Moreover, there is no systematic alignment of onshore and offshore channel systems. The nearshore data gap prevents an estimate of the possible contribution to offshore runoff from the small onshore catchments, and there is no published hydrometric data for these catchments. Here, we treat the offshore channel systems as fully decoupled from the onshore systems. The validity of this assumption remains to be tested with improved bathymetric data for the shelf. Furthermore, we assume that the channel systems are located in the same sequence of rhythmites and Luzon volcaniclastics that dominate the Coastal Range onshore. The main channels are V shaped with a small amount of sediment fill lining the base (Figure 6). In the onshore Coastal Range, we have also selected four catchments (Figure 5). They are slightly smaller with stream lengths of 8–15 km, and drainage areas of 40 km^2 to 60 km^2. For comparison, we have studied the catchment of the Liwu River, in the Central Range. Here, the main channel length is ~70 km and the drainage area is ~600 km^2. This catchment is located in medium to high-grade metasediments of the Pilushan and Tananao Formations. For each of these channel systems, we have compiled information on the long profile shape of trunk and tributary channels, the magnitude of local slopes, and the slope-area and curvature-area relationships.

5.3. Longitudinal Channel Profiles

[31] The longitudinal profiles of the trunk streams of the Liwu and Coastal Range catchments are taken from

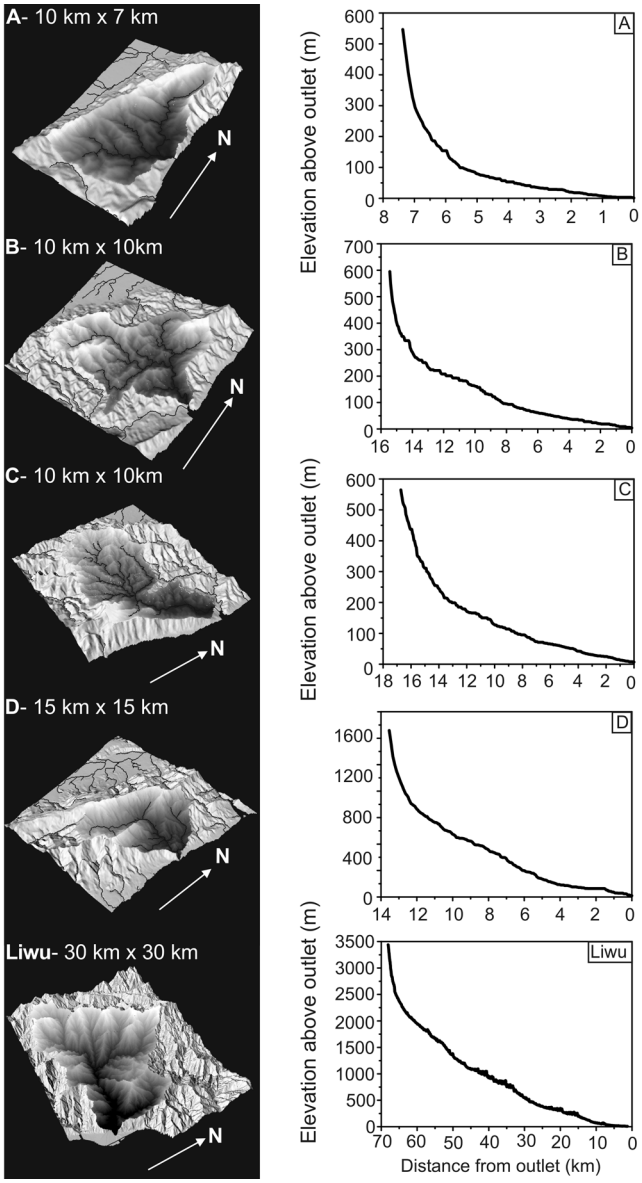

Figure 7. 40 m DEM of each onshore basin. The extent of each block is given. For the locations of the basins, see Figure 5. The elevation has two times vertical exaggeration and includes the streams with a catchment area greater than 1 km^2. The corresponding trunk stream profiles are generally concave but have several short convex sections and complexities; these are particularly notable in the larger Liwu catchment.

the 40 m filled DEM. The profiles are generally concave up (Figure 7), but they exhibit a number of complexities in detail. In particular, the longer Liwu profile shows a number of short (10^{-2}–10^{-1} km) convex-up sections and knickpoints. These are assumed to mark the locations of anomalously resistant rock outcrops, recent landslide blockages, and/or spatial variations in uplift rate or discharge, but some may be artifacts of our flow routing procedure. The channel profiles of the smaller Coastal Range streams contain more broad convex-up sections that make up about 10–20% of the overall channel relief. These are especially distinct in basin D where the trunk stream profile has a broad convex-up section as well as a small, sharp knickpoint at the basin outlet. Basin D is elongated along the structural grain of the Coastal Range (Figure 7, plot D and DEM and Figure 5) and cuts eastward to the coast through a narrow outlet gorge. In all five onshore catchments, most tributary streams have concave-up long profiles that commonly grade into the trunk stream (Figure 8), although straight or convex, and hanging tributaries do occur.

[32] The long profiles of submarine channels are taken from the 100 m filled DEM and are more variable in form

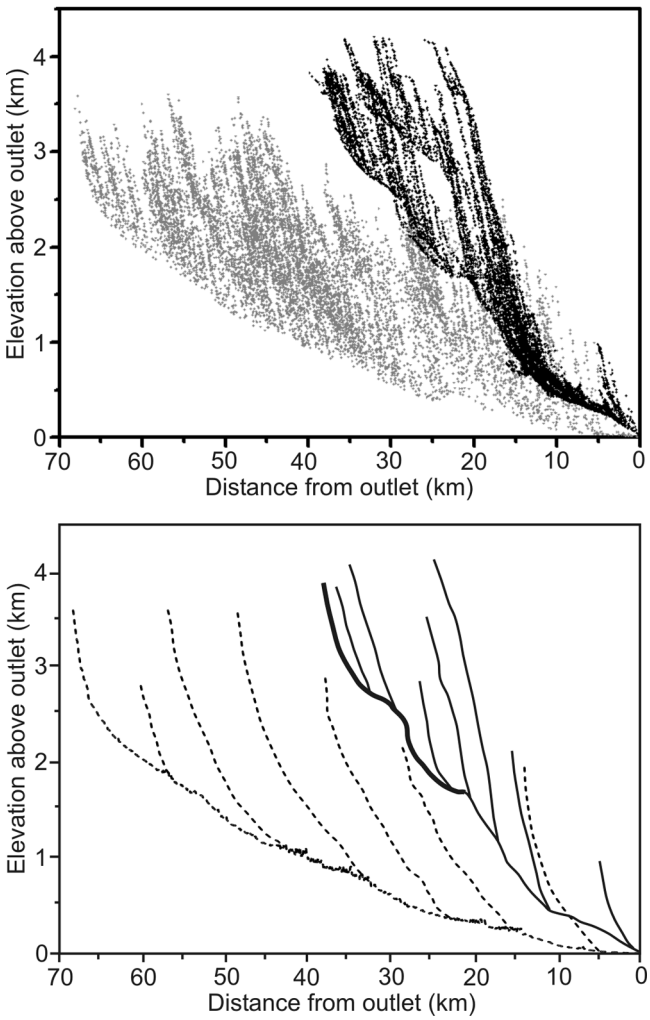

Figure 8. Elevation data from the drainage network of the Liwu basin (light gray) and basin G offshore (black). The raw data are given in the top plot, and the traces of the main trunk streams and several tributaries are given in the bottom plot. The Liwu profile is concave up with several small complexities and convex sections that are a small proportion of the total relief. The tributaries are concave and grade into the main channel. The data from channel G continue to the base of the shelf to provide a comparable length profile to the Liwu basin. The portion of profile G shown in Figure 9 is traced in bold. The main trunk stream has concave-up sections disrupted by significant convexities that are a greater proportion of the total relief than is seen onshore. The tributaries are straight and steep and abruptly merge with the main channel.

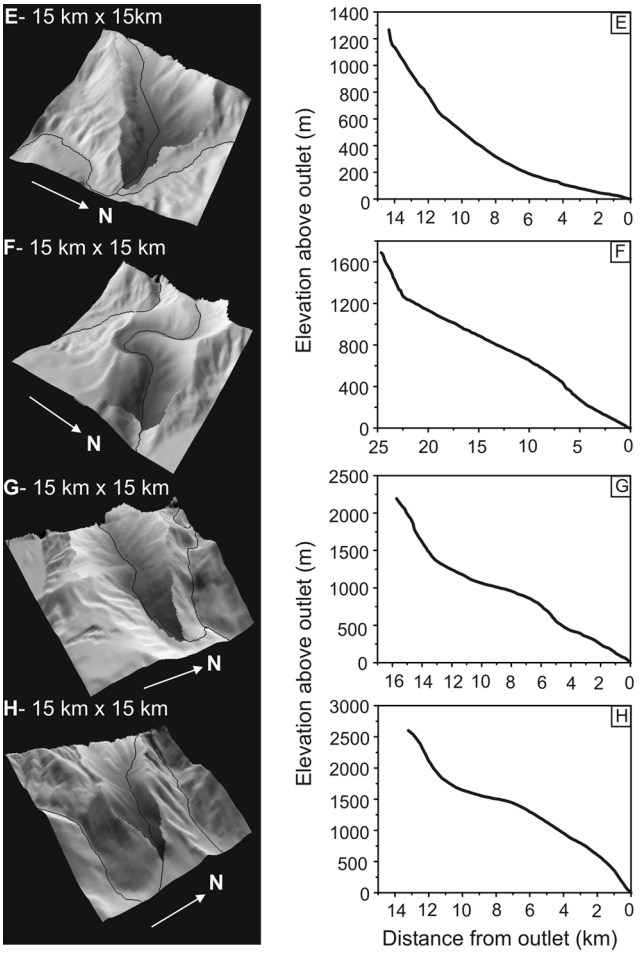

Figure 9. 100 m DEM of each offshore basin. The extent of each block is given. For the position of the basins, see Figure 5. The elevation has two times vertical exaggeration and includes the main trunk streams as a thin black line. The corresponding profiles are varied in form but are, in general, straighter than onshore with large convex-up sections.

(Figure 9). Only one out of four submarine channels in our study has a concave-up shape, conforming to the subaerial norm. The lower reaches of the long profiles of basins G and H are dominated by broad convex-up sections with a length of up to 10 km, and a departure of up to 500 m from a hypothetical, concave-only profile. The profile of channel F is particularly unusual. The main channel exhibits several kilometers of relief yet retains a constant slope of 3–4° for its entire length with only minor deviations at the outlet and headwaters. The DEM of basin F reveals well developed, valley meanders akin in form to onshore channel systems. When compared with the subaerial valleys, the submarine channels have relatively few tributaries and small-scale complexities in channel profile, although this may be a consequence of the lower-resolution DEM. The tributaries are generally straight, and steep (20°–22°) and merge abruptly with the main channels (Figure 8).

[33] It is more difficult to extract information on channel cross-sectional shape from our topographic data. On land, channel widths are typically narrower than the smallest grid cell (40 m). However, we know from field visits that valleys are commonly V shaped with a rectangular inner gorge and/or parabolic valley floor [e.g., *Hartshorn et al.*, 2002]. The DEM of offshore catchments E, F, G and H shows flat channel floors up to 1 km in width. Seismic line ACT36 (Figure 6) suggests that these flat channel floors are due to aggradation of an otherwise V-shaped bedrock channel. Such fills, in an otherwise erosional landscape, are likely due to overwhelming sediment supply from adjacent hillslopes, or sources higher in the channel system, and/or downstream tectonic or slide blockage of the valley. This sediment must be stripped away before lowering of the bedrock channel floors can occur.

5.4. Slope Statistics

[34] Next we turn to the geometry of the valley sides. We have calculated the slope of steepest descent at each grid point in the nine channel systems and compare the catch-

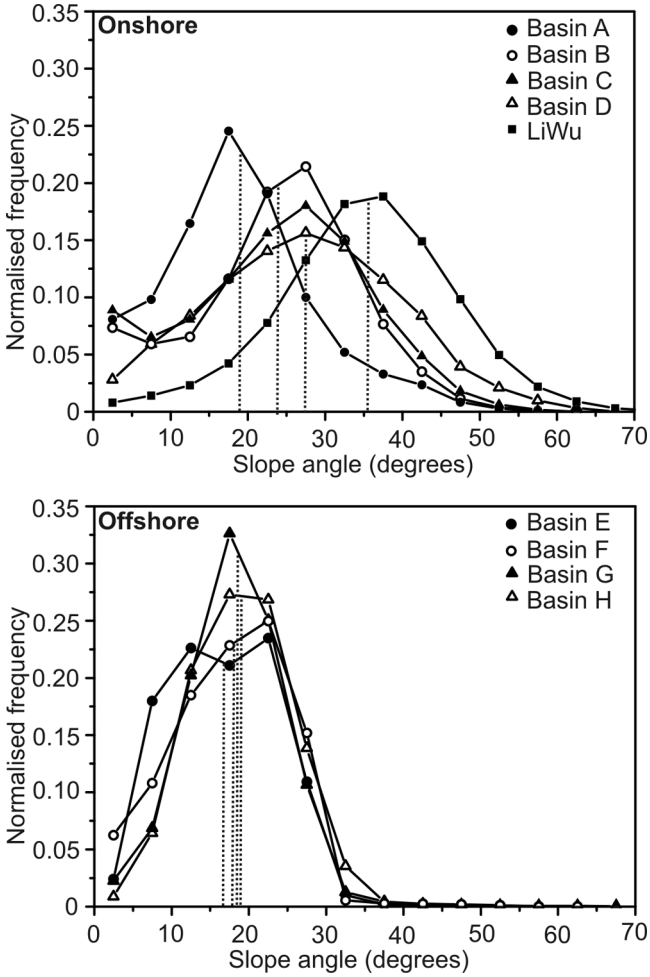

Figure 10. Slope frequency plots for the (top) five onshore basins and (bottom) four offshore basins. The slopes have been binned at 5° intervals, and the frequency has been normalized by basin area. The mean slope of each basin is shown by a dotted line. Basins B, C, and D and the Liwu basin show a broad peak with a modal value close to rock strength tests. Offshore, basins E, F, G, and H show a much narrower distribution of slopes and of mean slope estimates.

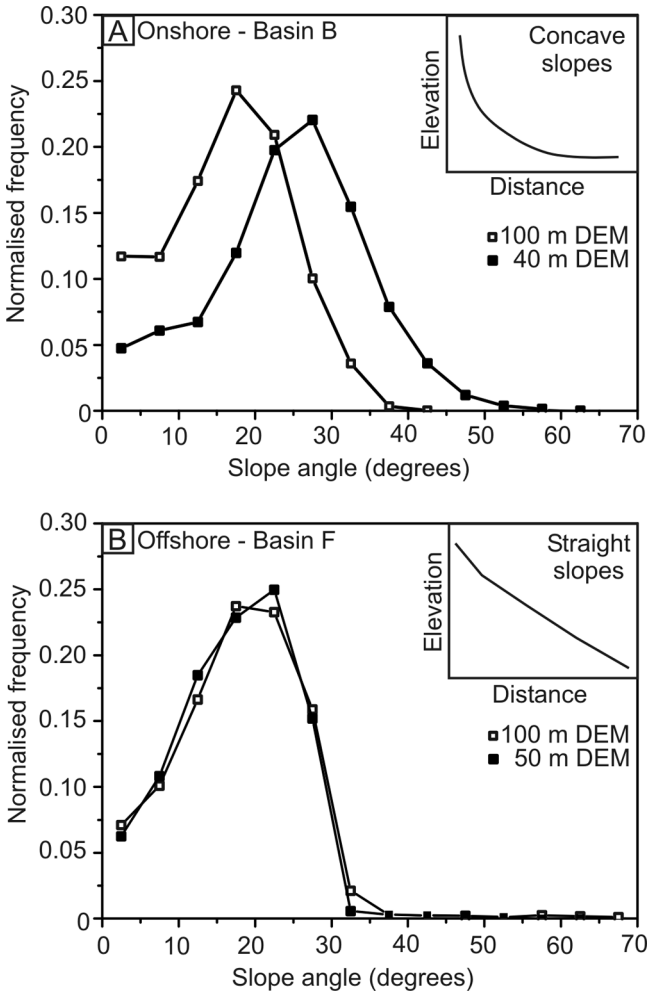

Figure 11. (a) Slope frequency plots for basin B from the 40 m DEM (solid squares) and from the 100 m DEM (open squares). Note how the modal peak shifts to a lower value as the resolution of the DEM decreases. This is a result of resampling the typically concave-up slopes onshore. (b) Slope frequency plot for basin F from the 50 m DEM (solid squares) and the 100 m DEM (open squares). Note how the modal peak is almost identical. This may be a result of resampling the much straighter hillslopes offshore.

ment-wide slope frequency statistics. Slope statistics are dominated by locations with small upslope areas, that is, the hillslopes. Any differences between the onshore and offshore slope statistics are likely due to differences in hillslope characteristics. The flat valley floors of the submarine channels (see above) produce a strong modal peak at a low topographic slope. We have eliminated these flat floors from our analysis by manual delineation from the DEM because we are now interested in the hillslopes. Analysis was carried out on the catchment as a whole, on the valley floors only and as the difference between the two. The slope calculation was performed at the highest resolution of the subaerial and submarine digital elevation models (40 m and 100 m, respectively) and length-scale issues will be discussed below.

[35] Slope frequency plots for the four onshore Coastal Range catchments (Figure 10) all show a broad spread around a modal value of ~28°, with the exception of catchment A which has a similar spread but a lower modal value of 18°. In all four catchments local slopes steeper than 35° are common, and slopes as steep as 60° are found. The Liwu basin has a higher modal value of slope at ~35° but shows the same broad spread of data. This is in sharp contrast with the nearby submarine channel systems, that have narrow, unimodal slope frequency distributions with a strong peak at 18°–20°, and very few locations steeper than 35°. Basin E has the same narrow range of common slope values, but a less pronounced modal peak than the other submarine channel systems.

[36] Clearly, slope measurements are strongly dependent on length scale and the digital elevation model resolution. *Stark and Stark* [2001] have shown that slope values asymptotically approach stability at higher DEM resolution. It is not clear at what length scale a robust approximation of the real local slope is obtained and how this length scale may vary between landscapes with differing boundary conditions. In the absence of very high resolution DEMs for onshore and offshore Taiwan, we cannot address this issue here. However, we have recalculated the slope frequency statistics of the onshore Coastal Range catchments using the 40 m DEM resampled at 100 m resolution. As expected, the modal peak in slope frequency of the coarser resolution data has shifted to a lower value of 18° (Figure 11). Therefore we cannot assert with any confidence that the 40 m DEM provides a real local slope estimate onshore. A similar test is more difficult offshore, but we obtained 50 m resolution bathymetric data for a shallow water segment of channel system F. We found that the slope frequency statistics are almost identical at 50 m and 100 m resolution, at least for this channel system (Figure 11). We conclude that, perhaps surprisingly, the 100 m offshore DEM may provide true local slope statistics. We believe that the difference in behavior of the onshore and offshore slope statistics may be the effect of resampling the more concave subaerial landscape, as opposed to the more planar, less dissected submarine landscape (see section 5.6).

[37] In the absence of higher-resolution data, we must accept that the slope statistics calculated from the available DEMs at the highest possible resolution provide the best achievable approximation of real slope statistics. We cautiously proceed in our interpretation, but we are aware that the modal values of topographic slope may not be truly representative of hillslope angles.

5.5. Slope-Area Relationship

[38] In this section, we explore the dominant erosional processes in the onshore and offshore environment using slope-area relationships from each of the nine catchments (see section 2). The slope-area data are used as an independent tool for characterizing the network morphology and do not imply any steady state assumption with regard to the submarine realm. As before, the slope was calculated along the path of steepest descent (i.e., in the direction that water/sediment would follow), and the drainage area was defined using an algorithm of steepest slope flow routing. We present slope-area data for catchments rather than for single

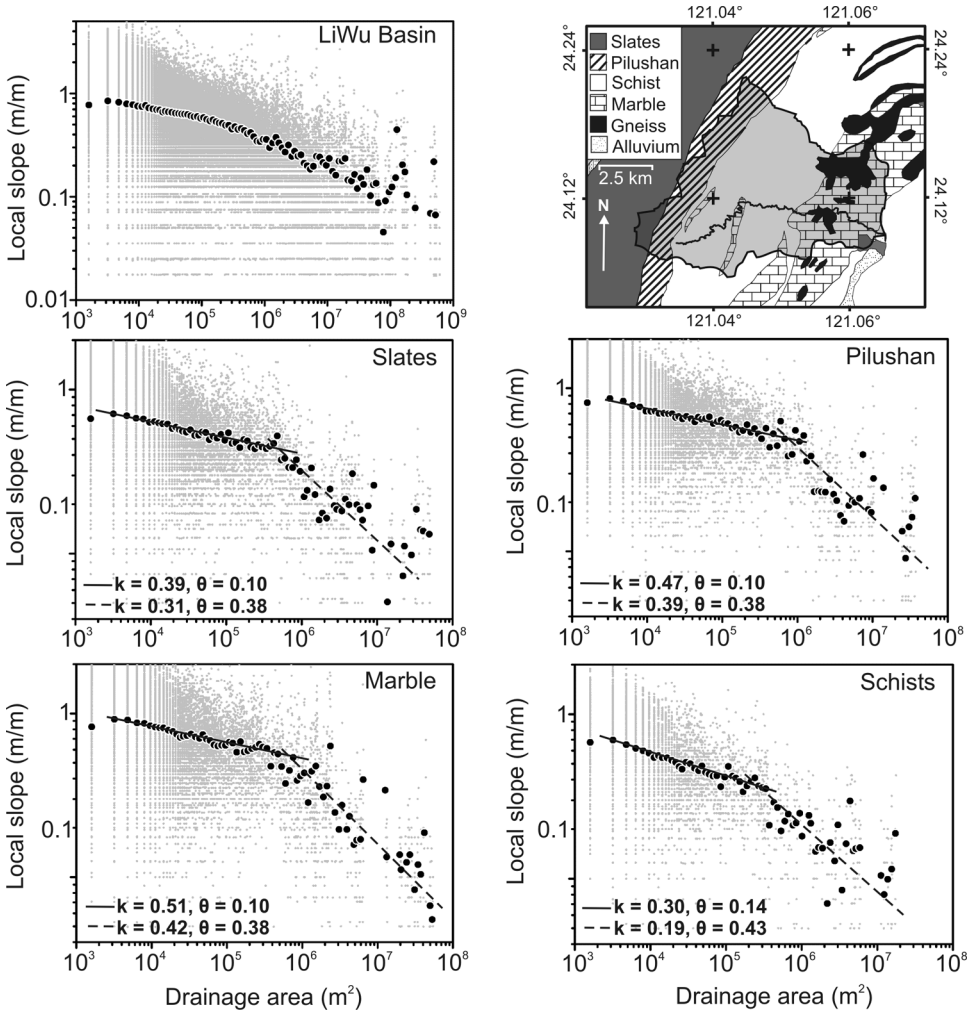

Figure 12. Slope-area plot for the entire Liwu basin. Raw data are shown in light gray, and the logarithmic binned mean is shown in black. There is a gradual scaling between local slope and drainage area with no clear break in process domain. The Liwu basin is composed of a number of lithological units as shown by the geology map. The slope-area plots of single lithology subcatchments of the Liwu basin show two distinct process domains, a landslide domain where $\theta \sim 0.10$ and a fluvial domain where $\theta \sim 0.40$. The same pattern is shown by all four lithologies, although the break in scaling occurs at a different threshold area.

channel profiles. Amalgamation of many channel profiles catchment-wide may lead to a smearing of trends and transitions but removes uncertainties associated with the selection of individual channel profiles. The slopes were averaged in equally spaced logarithmic bins and the slope-area parameters fitted using a least squares algorithm where appropriate. The analysis was carried out using the highest resolution DEM in the subaerial and submarine realms (i.e., 40 m and 100 m respectively). Both the mean slopes and the raw data are presented in log-log space in Figures 12, 13, and 14. We review our observations and offer some initial interpretations. Further interpretations and discussion will follow in a later section.

[39] The slope-area relationship for the Liwu basin shows a gradual change of scaling, without a clear breakpoint (Figure 12). The heterogeneity of such large basins, in terms of lithology, rainfall, water discharge and rock uplift, might obscure any clear process domains. In an attempt to address this issue, we have performed slope-area analyses for smaller subcatchments with uniform lithologies [cf. *Lague et al.*, 2000]. We note that heterogeneities in uplift rate and discharge may still exist for these smaller catchments, as well as lithologic variation between and within the beds of any given formation, but we have no information from which to constrain this smaller-scale variability. We have identified four significant lithologic units within the Liwu catchment: marbles, schists, the Pilushan Formation (slate and phyllite) and the Lushan Slates. We present a summary of our lithology-specific results in Figure 12.

[40] All four lithologies have clearly defined slope-area relationships with an almost horizontal trend ($\theta = 0.1$) for locations with small upslope areas, and a scaling exponent, θ, between 0.38 and 0.43 for larger areas (Figure 12). A low scaling exponent is thought to be typical of landslide failure that sets hillslopes to an almost constant angle over a range of length scales. A scaling exponent of $0.3 < \theta < 0.6$ is

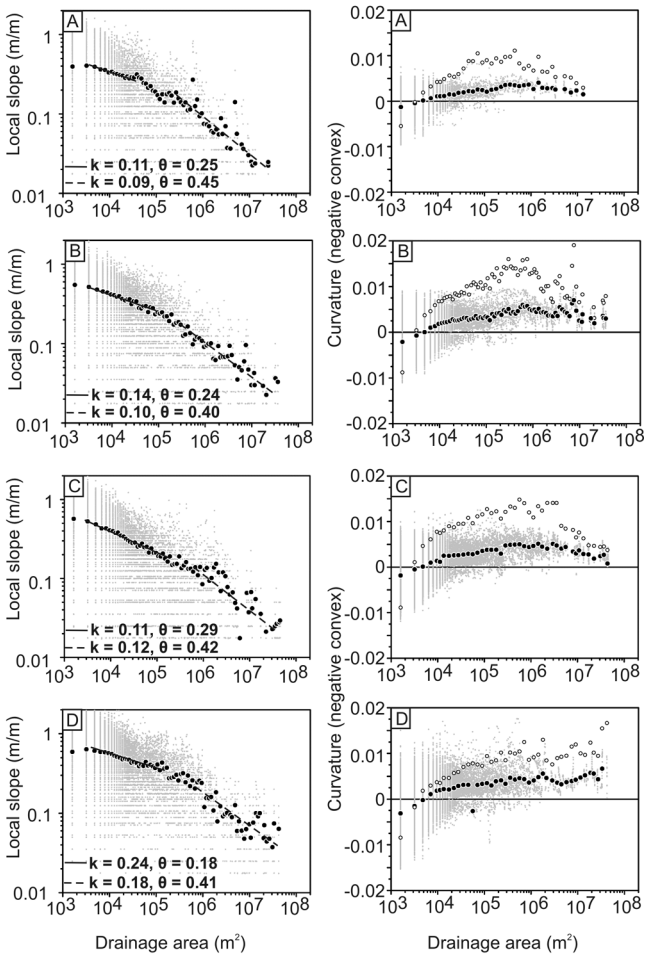

Figure 13. Slope-area and curvature-area plots for Coastal Range basins A, B, C, and D. The data for the slope-area plots are taken from the 40 m onshore DEM; the raw data are shown in light gray, and the logarithmic binned mean is shown in black. Generally, slope decreases gradually with increasing drainage area, and it is difficult to identify clear process domains. We have estimated θ to lie between 0.2 and 0.3 for the initial small drainage areas, a value too high for landslides and too low for fluvial domains. We have also calculated curvature in a 3 × 3 window for the 40 m DEM (open circles) and the 100 m DEM (solid circles). Both data sets show a negative (convex) curvature at low-drainage areas, such as ridge crests, and an increasing concave curvature at increasing drainage areas. Compare with Figure 14.

thought to be characteristic of fluvial channels [*Whipple*, 2004]. The transition between the landslide and fluvial domains occurs at an upslope area of around 0.3 km^2 to 1.0 km^2, dependent on lithology. We attribute the gradual change of slope-area scaling for the entire Liwu catchment primarily to the superposition of the individual lithologic slope-area relations, although variations in uplift rate and discharge will also play a part.

[41] The slope-area plots for the onshore Coastal Range catchments (Figure 13) also show a gradual change of the scaling behavior across all length scales. These catchments are small in comparison to the Liwu, and we might expect any variation in uplift rate and specific runoff to be limited. Nevertheless, radiometric dating of marine terraces along the eastern coast has documented an increase in Holocene surface uplift rates from 3–4 mm/yr in the north to 6–9 mm/yr in the south [*Hsieh et al.*, 2004]. Tilting and warping of the marine terraces and dating of sites landward also suggest a slight increase in uplift rate from east to west [*Hsieh et al.*, 2004]. Furthermore, several thrust faults run along the Coastal Range and cut across basins B and C, although the activity and role of these faults in the Holocene is a matter of debate. The lithology in the catchments is variable but not on the scale of the Liwu. Of the basins we have chosen, B and C are largely (85–95%) underlain by the Takangkou Formation, a 3–4 km thick sequence of Plio-Pleistocene sandstone and mudstone rhythmites, and

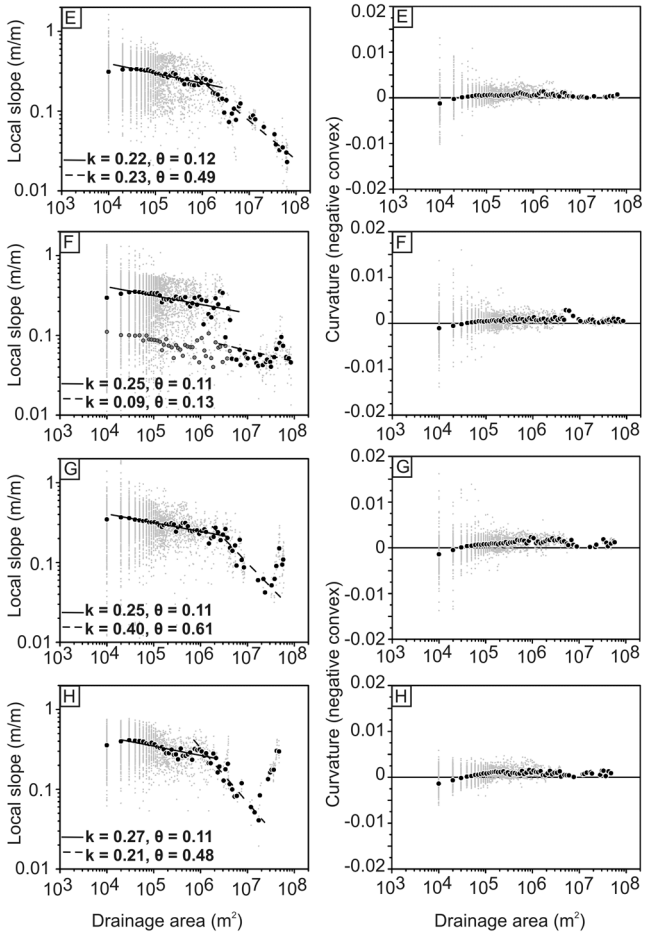

Figure 14. Slope-area and curvature-area plots for basins E, F, G, and H. The data for the plots are taken from the 100 m offshore DEM, and the flat valley floors visible in the DEM have been removed (see text for details). Basin F includes the valley floor data in medium gray. Generally, two clear topographic signatures are distinguished for each offshore basin, a signature with a low scaling exponent (θ ∼ 0.1) and a signature that overlaps in form with the onshore fluvial domain, where θ lies between 0.3 and 0.6. We have calculated curvature in a 3 × 3 window for the 100 m DEM. The curvature is consistently low at all length scales, a result of the poorly dissected landscape and straight slopes seen offshore.

volcanic detritus deposited in a submarine slope setting. The Tuluanshan Formation comprises andesitic tuffs and associated agglomerates and sediments. These volcanics outcrop in the remaining lower reaches of basins B and C and underlay most of basin D (75%). The headwaters (25%) of basin D are composed of the Takangkou Formation. In basin A the Tuluanshan and Takangkou formations are present in roughly equal proportions, with alluvium in the lower reaches. Despite these lithological differences, the slope-area signature of all four basins is very similar. For this reason, we believe that the curved slope-area relationships are not an artefact of geological heterogeneity of the catchments, but more likely a result of varying uplift rate, discharge or the manifestation of the erosional process itself. For drainage areas <0.5 km^2 the scaling exponent, θ, is around 0.25 in all cases (Figure 13). In general, there exists no tightly defined set of θ values that differentiates one erosional process from another, but a θ of 0.25 is probably too high for landslides, and too low for fluvial channels, and may instead reflect the presence of a fine network of debris flow channels [cf. *Lague and Davy*, 2003; *Stock and Dietrich*, 2003]; see section 6). At larger upslope areas all four basins have a power law relationship between slope and area with an exponent close to 0.4.

[42] Offshore, all four catchments show two clear topographic signatures and, surprisingly, are more comparable in form with the catchments of the Liwu than with those of the Coastal Range (Figure 14). In basins E, G and H a domain with slow, but systematic decrease of local slope with increasing upslope area ($\theta = 0.1$) is separated from a domain with a uniform scaling exponent, $0.48 < \theta < 0.61$, by a crisp break in scaling behavior at 1–3 km^2 upslope area. We note only the statistical similarity of these topographic signatures to the landslide and fluvial process domains observed in subaerial river systems and will discuss the implications of this observation later. The domain with a low slope-area exponent has a greater downslope extent offshore than onshore in the Central Range and gives a characteristic local slope of $\sim 20°$ at 0.01 km^2 upslope area in all cases.

[43] In general, the four offshore catchments share a common pattern with the distinct division of two topographic signatures, but there are a number of important digressions. Catchments G and H are concave up in their upper reaches but have large convex-up sections in the lower 10 km of their longitudinal profiles (Figure 9). These knickpoints are reflected by 'tails' of increasing slope with increasing upslope area at 10–20 km^2. We consider that $\theta \sim 0.5–0.6$ is characteristic scaling for the submarine channel systems of east Taiwan, and that the deviation from this behavior for large upslope area in basins G and H is due to local conditions. The channel profile of catchment F is distinctly linear (Figure 9) and results in a second almost horizontal trend in the slope-area relationship at large upslope areas.

5.6. Curvature-Area Relationship

[44] To obtain additional information on the dissection of the landscape below the channel threshold, we have calculated the maximum local curvature of the topography in a 3 by 3 window at varying resolution and plotted values against upslope area in linear log space (Figures 13 and 14). In most cases, maximum curvature is not found along the line of steepest descent, but perpendicular to it. The plotted curvature then reflects the presence of channels, and the spacing and steepness of adjacent valley sides. Removal of the flat valley floors from the bathymetric data makes no fundamental difference to the curvature results.

[45] Measured from the 40 m DEM, the topography of the subaerial Coastal Range catchments is concave everywhere, except at convex ridge crests (negative curvature at very small upslope areas). We have repeated our curvature analysis of the Coastal Range catchments with the DEM resampled at 100 m pixel size to match the resolution of our offshore data. At this resolution, the overall pattern of curvature is maintained, but the curvature values are less extreme (Figure 13). Concavity values peak at 1–3 km^2 upslope area, and decrease into the fluvial domain. This may be due in part to the increased likelihood of channel widths greater than the length scale at which we have estimated curvature.

[46] Offshore, curvature is consistently low for all upslope areas and considerably less than the curvature of onshore data at both the 40 m and 100 m resolution DEM. Although at larger upslope areas this may be due to the presence of valley fill, or to the fact that we are measuring curvature at a scale smaller than the valley width, this is not the case for smaller upslope areas. We infer that a lack of dissection of slopes with upslope areas of less than 1–3 km^2 is the cause of low curvature at small upslope areas.

6. Interpretations and Discussion

[47] There are a number of limitations to the geomorphic study of the submarine landscape. The obvious lack of ground truthing, compared with subaerial geomorphology, makes any proposed interpretation difficult to test. There are no available borehole data for the submarine slope off the east coast of Taiwan, and the lack of constraints on lithology makes it necessary to extrapolate observations and measurements made onshore. The water depth places a limit on the maximum resolution of the digital elevation model and does not permit the fine-scaled analyses that can be pursued on land. Finally, we have no other remotely sensed data to complement the bathymetric data set and cannot observe the erosional processes firsthand. Acknowledging these limitations, we embark on an interpretation of our results by comparison with present knowledge of subaerial geomorphology, and we attempt to link these inferences to formative erosional processes offshore.

[48] One of the most striking results is the existence of clear topographic domains in the submarine environment. Moreover, these offshore domains are directly comparable in form to those found in subaerial landscapes. Although it is not possible to characterize the nature of the formative process from knowledge of the slope-area scaling behavior alone [*Whipple*, 2000; *Whipple and Tucker*, 2002], we consider the likely erosional processes at small and large upslope areas before turning to a more general discussion of the results.

6.1. Potential Erosional Processes at Small Upslope Areas

[49] A slope-area scaling exponent of 0.1 is observed for small upslope areas in both the submarine channel systems

and the Liwu catchment (Figures 12, 13, and 14). A low scaling exponent suggests a process capable of setting a near constant slope over a range of length scales. The widespread existence of a modal slope is reiterated for all basins in the statistics of topographic slope at the mountain belt (Figure 3) and catchment scales (Figure 10). Elsewhere, strong modal peaks in slope frequency plots have been interpreted to reflect the maximum stable slope permitted by the geomechanical properties of the substrate. In other words, the modal peak is seen as the critical slope for threshold processes such as bedrock landsliding [*Burbank et al.*, 1996]. Infinite slope analysis [e.g., *Selby*, 1993] predicts that the threshold slope angle is equal to the angle of internal friction, θ, for dry rock rubble, and that the threshold slope angle is reduced for saturated conditions when seepage is parallel to the slope and the water table is at the surface.

[50] The metasediments of the Liwu typically have friction angles between 30–35°, dependent on specific lithology (H. Chen, personal communication, 2004). These values are in close agreement with calculated modal slope. With the assistance of ground truthing, we can confidently attribute the low scaling exponent for small upslope areas ($A < 1$ km^2) in the Liwu to erosion of the hillslopes by landslides. Independent confirmation comes from the pervasive nature of landsliding documented elsewhere in the eastern Central Range [*Hovius et al.*, 2000]. However, the case for the Coastal Range and offshore data is less clear cut. The sedimentary and volcaniclastic rocks of the Coastal Range commonly have an angle of internal friction of $\theta = 25°$, but with significant local variation dependent on specific lithology (H. Chen, personal communication, 2004). These experimental values are similar to the modes of our onshore slope frequency analyses and landsliding may be an important process at low-drainage areas, but this is not reflected in the curved slope-area relationships (Figure 13). The lower modal and mean slope of basin A may be attributed to the more extensive presence of weak mudstone horizons at this locality and/or the existence of hillslopes below the mechanical threshold of the substrate. The lower rock uplift rates at the northern tip of the Coastal Range [*Hsieh et al.*, 2004] make either interpretation probable. At present we do not have the detailed field information required to declare on this issue with any certainty.

[51] Offshore, we have found the modal slopes to be consistently lower at ~18–20°. We would expect the subaerial slopes and submarine slopes to be set by the same threshold value but there are several possible reasons for this lower modal slope. (1) The hillslopes have not reached their threshold because of rapid erosion rates or low uplift rates offshore. (2) The submarine slope is composed of a significantly weaker material than the subaerial Coastal Range with a lower friction angle. (3) Seepage has reduced the friction angle of the submarine substrate significantly. (4) The slope measured from the 100 m DEM is not a true representation of the hillslopes and the modal slope would increase to values similar to the Coastal Range for higher-resolution bathymetric data. Suggestions 1 and 2 seem unlikely given the proximity of the offshore basins to the onshore Coastal Range but cannot be ruled out without further investigation. Suggestion 4 cannot be entirely ruled out despite our analysis of the 50 m offshore data for basin F.

[52] As noted previously, the low scaling exponent in the submarine channel networks is similar in form to the landslide domain observed onshore, and it is tempting to suggest that landslides dominate offshore at low upslope areas. Landslides are known to be an important offshore erosional process, and this interpretation does not seem unreasonable. However, given the lack of direct observational data and the possibility of acausal relationships between slope and drainage area [*Schorghofer and Rothman*, 2001, 2002], we cannot be certain. Nevertheless, we think that it is probable that (bedrock) landslides limit the steepness of valley sides both on land and offshore, and that the substrate has very low cohesion at length scales relevant to landsliding. The departure of the slope-area scaling exponent from an absolutely horizontal trend, $\theta = 0$, may be related to increasing material weaknesses with increasing length scales [*Schmidt and Montgomery*, 1995]; the competition between landslides, debris flows and channel processes [*Tucker and Bras*, 1998]; spatial variations in pore pressure [*Montgomery and Dietrich*, 1994] and/or a progressive transition from dry landsliding at short length scales to saturated landsliding at longer-length scales (in the onshore case) [*Tucker and Bras*, 1998].

[53] Important differences between the subaerial and submarine topography are illustrated by the breadth of the slope frequency distributions (Figure 10) and the maximum-length scale to which the weak slope-area scaling dominates the topography (break in slope-area scaling behavior in Figures 12, 13, and 14). The slope frequency distributions of the onshore channel systems are broad and significant proportions of the topography are at subcritical or supercritical slopes. We suggest that the relatively broad spread of topographic slope values onshore is the result of geological and environmental heterogeneity of the catchments. For example, slopes may be stabilized above their mechanical threshold by dense vegetation, and slopes may fail below their threshold because of water accumulation at the slope toe resulting in increased pore pressures and/or increased weathering. We know of few environmental factors to increase the stability of submarine slopes and supercritical slopes are apparently removed quickly and effectively. Likely triggers of submarine slope failure include sediment loading on the shelf and seismic shaking, as well as the progressive lowering of channels at the toe of slopes. We have not investigated the depth dependence of offshore modal topographic slopes, but note that the tightness of the slope frequency distributions for seafloor topography spanning depth ranges of 1.5–2.5 km precludes a strong depth control on slope stability in our examples.

[54] In the competent metasediments of the Liwu catchment, landslides appear to occur in all lithologies up to an upslope area of ~1 km^2, but a break in the slope-area scaling occurs at a smaller-length scale in fissile schists and slates than in more massive carbonates and sandstones. Offshore, the domain with a low slope-area scaling exponent ($\theta \sim 0.1$), similar to landslide dominated areas in the Liwu, extends to upslope areas of 1–3 km^2. Thus offshore hillslopes are longer than in the Liwu catchment. As a result, the density of channels is less offshore than in the Liwu catchment and other onshore channel systems. In the

sediments and volcaniclastic rocks of the subaerial Coastal Range, very low slope-area scaling exponents are found only at locations high in the catchments with upslope areas of less than a few thousand m^2 (50 m equivalent length scale), where small-scale landsliding may dominate. However, it is difficult to distinguish the effect of landslides in such locations from the effect of measuring topographic slope across a ridge crest, and we do not place emphasis on these observations.

6.2. Potential Erosional Processes at Larger Upslope Areas

[55] In general, the slope-area scaling of the Coastal Range has no distinct scaling breaks but a gently convex-up continuous curve. This could be attributed to variations in uplift rate and/or discharge, but a third possibility is that the scaling is characteristic of the erosional process itself. Debris flows are known to be important erosional agents in steeplands where sediment is readily available, and several authors have identified the signature of debris flow channels in their catchment wide [*Lague and Davy*, 2003] or single channel profile analyses [*Stock and Dietrich*, 2003]. While there exists no consensus on the exact form of this topographic signature and no accepted debris flow incision law *Stock and Dietrich* [2003] observe that linear power law trends at large drainage areas tend to overpredict valley slope above 0.10 (5°) and give way to a nonlinear relationship between slope and drainage area in log-log space. We note a similarity between their observations and our findings in the Coastal Range (Figure 13), although in our data the linear power law extends to slopes of 0.30. We suggest that debris flows may be an important erosional process in the Coastal Range, as they are elsewhere in Taiwan [*Stock and Dietrich*, 2003]. This claim cannot be substantiated without detailed fieldwork in the Coastal Range catchments, particularly as other erosional processes may play an important part (e.g., earthflow processes in mudstone-rich horizons). However, if true, the prominence of debris flows at intermediate-length scales in the Coastal Range may be due to extreme weatherability of the substrate and/or the fact that it dissociates completely into relatively small, transportable clasts upon failure.

[56] At larger upslope areas most channel systems show a concavity of $0.3 < \theta < 0.6$. On land, we attribute the concavity of river channels to the systematic downstream increase of water discharge, combined with a less than linear increase of channel width with discharge. Offshore, channel erosion is driven by sediment rich density flows, and it is hard to imagine how 'water discharge' would systematically increase downstream in submarine channel systems. It is more likely that sediment load increases with increasing upslope area, and that positions lower down in the channel system experience a higher frequency of erosive flows [*Mitchell*, 2004, 2005; *Seidl and Dietrich*, 1992].

6.3. Physics of Offshore Erosional Processes

[57] Here, we briefly outline the most prevalent types of sediment gravity flows on the submarine slope and qualitatively contrast their governing flow equations to the stream power river incision model. In doing so, we refer to the four distinct types of sediment gravity flows as recognized by *Dasgupta* [2003] and characterized by different sediment support mechanisms: turbidity currents, fluidized sediment flow, grain flow, and debris flows. Of these turbidity currents and debris flows are the most widely recognized and have received the most attention in the literature; we primarily consider these two flow types in our interpretation. In all cases, the driving force is gravity acting downslope on the sediment particles and water [*Middleton and Hampton*, 1973].

[58] Turbidity currents, by definition, are turbulent flows of a grain-fluid mixture in which sediment constitutes the relatively minor component (<10% by concentration [*Bagnold*, 1962]). The grains are completely dispersed within the fluid and are supported by the fluid turbulence. In contrast to riverine flow, the fluid turbulence is initially brought about by the suspension of sediment in the water resulting in a strong feedback between sediment entrainment and turbulent flow. Turbidity currents may be surge-like or continuous. Typically, they erode along the submarine slope before depositing sediment lower down, but they can deposit vertically aggrading levees along their length [*Peakall et al.*, 2000]. Mean velocity is dependent on the depth of the flow and the channel gradient and governed by an expression similar to the Chezy equation for open channel fluid flow [e.g., *Komar*, 1977; *Middleton*, 1966b; *Middleton and Southard*, 1984]:

$$V = \left[\frac{g(\rho_t - \rho)}{\rho_t}\frac{HS}{C_{D(t+b)}}\right]^{\frac{1}{2}} \tag{2}$$

where ρ_t is the current density, ρ is the overlying fluid density, H is the flow depth and S is the channel gradient, $C_{D(t+b)}$ is the drag coefficient at the top (t) and bottom (b) of the flow. The density contrast between the current and overlying fluid and the drag at the top and base of the flow are important controls on the velocity of the turbidity current and can change rapidly within a single flow. Nevertheless, the mean velocity is a power function of slope and flow depth, just as it is for mudflows, pure fluid flow, and riverine flows. Furthermore, turbidity current erosion can be expressed as a direct function of shear stress, and the shear stress at the base of the turbidity current scales with the square of the flow velocity [*Mulder et al.*, 1998; *Mitchell*, 2004], as it is modeled for rivers. For a less than linear relation between channel width and discharge, as in fluvial channels, and a distinct proportionality of discharge and down-channel distance, this expression would predict the formation of concave-up turbidity current channels with slope-area scaling similar to that of bedrock rivers [*Mitchell*, 2004]. However, there are several problems with this model, of which we highlight three. First, no systematic knowledge exists of the downstream evolution of the width of erosional turbidity current channels, and the assumption of less than linear scaling of width and distance cannot be substantiated at present. Secondly, the assumption of a systematic, down-channel increase of discharge is unlikely to apply to all turbidity currents. Many turbidity currents originate at a single point. This may be a submarine landslide, a channel head in a shelf through which suspended shallow marine sediments are funnelled, or the mouth of a river with hyperpycnal discharge (in which the density of the river discharge is greater than that of the receiving seawater). In

each of these cases, it may be more appropriate to assume a constant discharge rather than increasing discharge, unless the turbidity current entrains water and sediment on its way down the channel. Systematic down-channel increase of discharge is most likely to occur when flow is contributed from many sources distributed throughout a channel network. This would require simultaneous mass wasting throughout a channel network, the likelihood of which we do not know. Thirdly, it is known that flow within the head of a turbidity current is highly unsteady and nonuniform given the influx of sediment from the tail. The flow velocity at the head of the current is independent of slope [*Benjamin*, 1968; *Middleton*, 1966a; *Middleton and Southard*, 1984]:

$$V_h = C(g'H)^{\frac{1}{2}} \tag{3}$$

where g' is $\frac{g(\rho_t - \rho)}{\rho_t}$. If most erosion occurred in the head of the turbidity current we might not expect a strong dependency of channel slope on contributing area.

[59] Debris flows are high-density flows in which larger clasts are supported by a water-clay matrix, and not a turbulent fluid, and where momentum transport by solid grains may dominate. Debris flows are discrete events onshore and offshore, consisting of single or multiple surges that have a well-developed head and gradually tapering tail that is more dilute. Debris flows are often modeled as non-Newtonian laminar flows with a Bingham plastic rheology. However, the true rheology of debris flows is more varied [*Iverson and Vallance*, 2001] and concentrated grain-fluid mixtures can act as rigid plastic solids or flow like liquids depending on pore fluid pressure. *Marr et al.* [2001] observed the influence of the clay-water content on the coherence of experimental debris flows. High water content and low clay content produced poorly coherent mixtures that readily transformed to turbidity currents on the entrainment of fluid and dilution of the flow. Strongly coherent debris flows had high clay content and did not produce significant subsidiary turbidity currents. *Marr et al.* [2001] also recognized the importance of 'hydroplaning' in coherent debris flows whereby a thin layer of fluid separates the flow from the underlying slope preventing the transmission of shear stress to the substrate and, essentially, preventing erosion of the channel bed. Hydroplaning is widely recognized in submarine debris flows but is not necessarily an integral part of subaerial debris flows [*Mohrig et al.*, 1999]. Further work is necessary in scaling these experimental models and observations to the continental slope.

[60] As noted previously, in subaerial DEM analysis the slope-area relationship of channels primarily eroded by debris flows has been attributed a curved topographic signature [*Stock and Dietrich*, 2003], or a power law fit with a low slope-area exponent close to ~0.25 [*Lague and Davy*, 2003]. Neither of these observations fit our offshore data at large drainage areas and therefore two possible interpretations exist. (1) Debris flows have a range of topographic signatures in slope-area space, or at least a signature in the submarine realm that overlaps with the subaerial fluvial domain. (2) Debris flows are not the dominant erosive flow on the Taiwanese submarine slope, and turbidity currents (or some other sediment gravity flow) are potentially more important.

[61] Submarine debris flows are likely to be significantly different to their onshore counterparts given the difference in viscosity of the overlying 'fluid' (air in the subaerial case) and the greater chance of fluid entrainment offshore. In relation to our suggested interpretations, it is likely that submarine (and possibly subaerial) debris flows may have a range of signatures in slope-area analysis. The erosive potential of such submarine debris flows is yet to be quantified. Furthermore, debris flows and turbidity currents are two distinct members of a continuous range of sediment gravity currents and present a continuum of potentially erosive flow rheologies that may not have distinct topographic signatures. Moreover, the properties of any sediment gravity current are constantly changing as sediment or water are added to or subtracted from the flow and debris flows will readily give rise to turbidity currents further downslope (e.g., the Nice airport failure in 1979 [*Mulder et al.*, 1997]). There have been few attempts to measure directly the incisive nature of sediment gravity flows and we have no direct measure of offshore erosion rates.

[62] The concavity of submarine channels in Taiwan is likely to be complicated by lithological heterogeneity, variation in rock uplift rate and/or rock strength, as it is onshore. In addition, the role of sedimentary processes along the margin shelf is unknown. Although transfer of sediment from the subaerial Coastal Range into the small submarine channel systems discussed here appears to be limited, the Kuroshio Current carries significant amounts of sediment northward along the shelf [*Boggs et al.*, 1979]. Accumulation of this sediment in the tributaries of offshore channels, inflows and seepage at the channel head, and storm wave action may all affect the headwater geometry of the submarine channel systems. Moreover, the geometry and discharge of the large submarine canyons that are fed by onshore rivers will affect the fluid flow field in the offshore slope and, in turn, control the growth of surrounding submarine canyons [*Orange et al.*, 1994]. No equivalent variables exist subaerially and additional data are necessary to isolate the offshore topographic signatures. Furthermore, the channel fill imaged in the seismic data and viewed in the digital elevation model must be excavated before channel erosion can continue. The fill may be a transient phase between large-scale sediment gravity currents or a more long-term phase of aggradation.

[63] In summary, it is unclear what longitudinal channel geometry should be expected for turbidity currents or debris flows. An in-depth investigation of this issue is beyond the scope of this paper, but we recognize it as an outstanding challenge for future research.

6.4. Further Interpretation

[64] Next, we briefly consider some other observations on submarine channel geometry. The channel profile of basin F is remarkably linear and gives rise to two almost horizontal trends in slope-area space. The low slope-area scaling exponent at low-upslope area is similar to basins E, G and H and might be attributed to hillslope landslides. At larger upslope areas, a constant slope of 3–4° prevails independent of increasing upslope area, a value similar to the overall slope of the accretionary wedge. Perhaps, the constant slope is the result of a recent, larger-scale slope failure that has not yet been carved extensively by sediment

gravity flows. Alternatively, the phenomenon could be attributed to inflows at the channel head, a progressive downstream increase in rock uplift rate [*Kirby and Whipple*, 2001], or selective aggradation of an otherwise erosional channel profile.

[65] Finally, we consider the large convexities in the lower portions of the channel profiles of basins G and H (Figure 9) that appear as 'tails' of increasing slope with area on the slope-area diagram (Figure 14). There exist several possible explanations for these convexities. These include more resistant underlying rock units, landslide blockage and/or variation in uplift rate or sediment supply. At this stage, none of these explanations can be excluded. However, *Malavieille et al.* [2002] mapped several thrust faults from seismic data offshore eastern Taiwan; some of which are within the submarine slope and cut across basins G and H (Figure 5). The convex sections of longitudinal profiles G and H may be steepening where they cross the tips of these growing thrusts [*Kirby and Whipple*, 2001]. If true, the large size of submarine knickpoints, as compared with river knickpoints onshore in east Taiwan, may be attributed to less effective channel incision and/or higher rates of fault displacement offshore east Taiwan. The presence of large-scale, west dipping thrust faults in the steep submarine slope off east Taiwan, together with the continuity of the mean topographic slope across the shoreline strongly suggest that the submarine slope is an integral part of the Taiwan orogen. The pattern and rate of erosion of the submerged east flank of the orogen may have profound geodynamic consequences elsewhere in the mountain belt. It is clear from our study that the submarine topography of east Taiwan is shaped by erosional processes, and that these processes have caused the formation of kilometer-scale relief. Hence the submerged part of an orogen should not be seen as the static pedestal of a subaerial mountain belt, but rather as an integral part of the coupled tectonics-erosion system in an area of crustal shortening.

[66] We note that the Taitung and Hualien canyons do have smooth, concave-up profiles across mapped thrust structures. These canyons are the only two in east Taiwan to have received significant quantities of river sediment at hyperpycnal concentrations since river gauging started some three decades ago [*Dadson et al.*, 2005]. They are larger and deeper than any other bathymetric feature in east Taiwan, and we attribute the difference in size and smoothness between them and the smaller channel systems described in this paper to the possible impact of hyperpycnally driven turbidity currents and the entrainment of additional, subaerially sourced sediment. The Hsiukuluan River is the third large river draining eastern Taiwan (Figure 2) and does not, at present, discharge sediment at hyperpycnal concentrations to the ocean. Correspondingly, the submarine Hsiukuluan Canyon does not cut a steep channel floor but is undergoing considerable aggradation (Figures 2 and 6). An in-depth exploration of the geometry and dynamics of these large canyons is beyond the scope of this paper.

7. Conclusions

[67] In the sedimentary system sea level is not the absolute base level for sediment transport, many sediment routing systems exhibit several kilometers of relief offshore before deposition in the sedimentary basin. We have shown that the offshore emerging topography of Taiwan can be directly compared with onshore topography using a range of geomorphic criteria. The main offshore channels are concave and steep with prominent knickpoints and the valley bottoms are wide and flat because of sedimentary fill. The submarine channel networks appear to have a low channel density, and adjacent hillslopes are long and undissected. Tributary channels are straight and, do not grade to, but abruptly join with the main channel. This is superficially a very different landscape to the highly dissected, dendritic drainage networks and V-shaped valleys that dominate subaerially, yet we have documented a number of fundamental similarities.

[68] Through slope-area analysis we have found that the Central Range and submarine channel systems show two clear topographic signatures. At small upslope areas, a slope-area scaling exists similar in form to that of landslide dominated areas subaerially. Within this domain, many slopes appear to be poised at their mechanical threshold, and few steeper slopes exist, probably due to slope collapse. The landslide-like signature shows a gradual decrease in threshold slope with increasing upslope area because material weaknesses may become more important at increasing length scales and/or there exists a competition between landslide and channel processes. Offshore, at larger upslope areas, the slope-area scaling exponent is similar to that of the fluvial channel network onshore, and debris flows and turbidity currents are the likely formative erosional processes. It is not yet clear whether or not the slope-area scaling of the submarine channel systems of east Taiwan can be attributed to debris flows or turbidity currents, and their roles in the formation of submarine erosional topography remain to be quantified. Targeted coring of the limited sedimentary deposits along the channel floor and valley sides may help to differentiate between these flow end-members but coring of the flat basin floors, distant from the submarine slope, will not provide significant information about the nature of the flow on the slope itself. Further experimentation aimed at constraining the 'discharge' or sediment yield with increasing upslope area and observations of the erosional processes from high-resolution bathymetric data may go some way to unravelling the potential topographic signature(s) of sediment gravity currents.

[69] We have also found major differences between the topographic signatures of the Coastal Range and Central Range of Taiwan. The curved slope-area signature of catchments in the Central Range is primarily a result of geological heterogeneity and there is a well-defined length scale of transition between hillslope and channel processes for lithologically uniform domains. In the Coastal Range, a curved slope-area signature is found in more homogeneous substrate and landslides are apparently only important at small drainage areas. This may be related to variation in uplift rate, water discharge or the manifestation of the erosional process itself. Surprisingly, a landslide-like signature is important over a much greater length scale offshore in the same volcaniclastic material. The different styles of mass wasting are potentially a result of subaerial weathering and/or vegetation cover.

[70] Our claims cannot be substantiated until our lack of constraints on submarine erosion and its forcing is

addressed, and we can only interpret our data in light of current knowledge of subaerial erosion laws. The few offshore basins described here have shown some variation in form, and it is not clear which observations can be taken as the 'norm' and which are out of the ordinary. In order to progress in submarine geomorphology, and to an extent in the study of subaerial erosional mechanisms, we must characterize a wider range of offshore environments. Only by comparison of the topographic form of a range of slope settings, tectonic boundary conditions and sediment fluxes can we isolate the controls on submarine erosion.

[71] **Acknowledgments.** We would like to thank Hongey Chen of the National Taiwan University for assistance in rock strength measurements and Philippe Davy of Géosciences Rennes for use of GridVisual software. The manuscript benefited from exceptionally thorough reviews by J. J. Roering, G. E. Tucker, and K. X. Whipple and discussion with S. J. Dadson, J. A. Jackson, J. M. Turowski, and R. T. Walker. L.A.R. was supported by a NERC studentship. This is Cambridge Earth Sciences contribution ES.8327.

References

Adams, E. W., and W. Schlager (2000), Basic types of submarine slope, *J. Sediment. Res.*, *70*, 814–828.

Bagnold, R. A. (1962), Auto-suspension of transported sediment: Turbidity currents, *Proc. R. Soc. London, Ser. A*, *265*, 315–319.

Band, L. E. (1986), Topographic partition of watersheds with digital elevation models, *Water Resour. Res.*, *22*, 15–24.

Barrier, E., and J. Angelier (1986), Active collision in eastern Taiwan: The Coastal Range, *Tectonophysics*, *125*, 39–72.

Benjamin, B. T. (1968), Gravity currents and related phenomena, *J. Fluid Mech.*, *31*, 209–248.

Boggs, S., W. C. Wang, F. S. Lewis, and J. C. Chen (1979), Sediment properties and water characteristics of the Taiwan shelf and slope, *Acta Oceanogr. Taiwan.*, *10*, 10–49.

Buffington, E. C., and D. G. Moore (1963), Geophysical evidence on the origin of gullied submarine slopes, San Clemente, California, *J. Geol.*, *71*, 356–370.

Burbank, D. W., J. Leland, E. Fielding, R. S. Anderson, N. Brozovic, R. Reid, and C. Duncan (1996), Bedrock incision, rock uplift and threshold hillslopes in the northwestern Himalayas, *Nature*, *379*, 505–510.

Cacchione, D. A., L. F. Pratson, and A. S. Ogston (2002), The shaping of continental slopes by internal tides, *Science*, *296*, 724–727.

Carena, S., J. Suppe, and H. Kao (2002), Active detachment of Taiwan illuminated by small earthquakes and its control of first-order topography, *Geology*, *30*, 935–938.

Chough, S., and R. Hesse (1976), Submarine meandering thalweg and turbidity currents flowing for 4,000 km in the Northwest Atlantic Mid-Ocean Channel, Labrador Sea, *Geology*, *4*, 529–533.

Dadson, S. J., et al. (2003), Links between erosion, runoff variability and seismicity in the Taiwan orogen, *Nature*, *426*, 648–651.

Dadson, S. J., N. Hovius, H. Chen, W. B. Dade, J.-C. Lin, M.-L. Lin, M.-J. Horng, T.-C. Chen, J. Milliman, and C. P. Stark (2004), Earthquake-triggered increase in sediment delivery from an active mountain belt, *Geology*, *32*, 733–736.

Dadson, S. J., N. Hovius, S. Pegg, W. B. Dade, M.-J. Horng, and H. Chen (2005), Hyperpycnal river flows from an active mountain belt, *J. Geophys. Res.*, *110*, F04016, doi:10.1029/2004JF000244.

Daly, R. A. (1936), Origin of submarine canyons, *Am. J. Sci.*, *31*, 401–420.

Dasgupta, P. (2003), Sediment gravity flow—The conceptual problems, *Earth Sci. Rev.*, *62*, 265–281.

Davis, D., J. Suppe, and F. A. Dahlen (1983), Mechanics of fold and thrust belts and accretionary wedges, *J. Geophys. Res.*, *88*, 1153–1172.

Deffontaines, B., J.-C. Lee, J. Angelier, J. Carvalho, and J.-P. Rudant (1994), New gemorphic data on the active Taiwan orogen: A multisource approach, *J. Geophys. Res.*, *99*, 20,243–20,266.

Dietrich, W. E., C. J. Wilson, D. R. Montgomery, and J. McKean (1993), Analysis of erosion thresholds, channel networks and landscape morphology using a digital terrain model, *J. Geol.*, *101*, 259–278.

Driscoll, N. W., J. K. Weissel, and J. A. Goff (2000), Potential for large-scale submarine slope failure and tsunami generation along the U.S. mid-Atlantic coast, *Geology*, *28*, 407–410.

Duncan, C., J. Masek, and E. Fielding (2003), How steep are the Himalaya? Characteristics and implications of along-strike topographic variations, *Geology*, *31*, 75–78.

Dunne, T. (1980), Formation and controls of channel networks, *Prog. Phys. Geogr.*, *4*, 211–239.

Duvall, A., E. Kirby, and D. Burbank (2004), Tectonic and lithologic controls on bedrock channel profiles and processes in coastal California, *J. Geophys. Res.*, *109*, F03002, doi:10.1029/2003JF000086.

Ernst, W. G. (1983), Mineral parageneses in metamorphic rocks exposed in Tailuko Gorge, Central Mountain Range, Taiwan, *J. Metamorph. Geol.*, *1*, 305–329.

Farre, J. A., B. A. McGregor, W. B. F. Ryan, and J. M. Robb (1983), Breaching the shelfbreak: Passage from youthful to mature phase in submarine canyon evolution, in *The Shelfbreak: Critical Interface on Continental Margins*, *SEPM Spec. Publ.*, vol. 33, edited by D. J. Stanley and G. T. Moore, pp. 25–39, Soc. of Econ. Paleontol. and Mineral., Tulsa, Okla.

Flint, J.-J. (1974), Stream gradient as a function of order, magnitude, and discharge, *Water Resour. Res.*, *10*, 969–973.

Fulthorpe, C. S., J. A. Austin, and G. S. Mountain (2000), Morphology and distribution of Miocene slope incisions off New Jersey: Are they diagnostic of sequence boundaries?, *Geol. Soc. Am. Bull.*, *112*, 817–828.

Hack, J. T. (1957), Studies of longitudinal stream profiles in Virginia and Maryland, *U.S. Geol. Surv. Prof. Pap.*, *294B*, 45–80.

Hampton, M. A., H. J. Lee, and J. Locat (1996), Submarine landslides, *Rev. Geophys.*, *34*(1), 33–59.

Hancock, G., and G. Willgoose (2001), The use of a landscape simulator in the validation of the SIBERIA catchment evolution model: Declining equilibrium landforms, *Water Resour. Res.*, *37*, 1981–1992.

Hartshorn, K., N. Hovius, W. B. Dade, and R. L. Slingerland (2002), Climate-driven bedrock incision in an active mountain belt, *Science*, *297*, 2036–2038.

Heezen, B. C., and W. M. Ewing (1952), Turbidity currents and submarine slumps, and the 1929 Grand Banks (Newfoundland) earthquake, *Am. J. Sci.*, *250*, 849–873.

Hickman, J. B., D. V. Wiltschko, J. H. Hung, P. Fang, and Y. Bock (2002), Structure and evolution of the active fold-and-thrust belt of south-western Taiwan from Global Positioning System analysis, in *Geology and Geophysics of an Arc-Continent Collision, Taiwan*, edited by T. B. Byrne and C. S. Liu, *Geol. Soc. Am. Spec. Pap.*, *358*, 75–94.

Hilley, G. E., and M. R. Strecker (2004), Steady state erosion of critical Coulomb wedges with applications to Taiwan and the Himalaya, *J. Geophys. Res.*, *109*, B01411, doi:10.1029/2002JB002284.

Hovius, N., C. P. Stark, H.-T. Chu, and J.-C. Lin (2000), Supply and removal of sediment in a landslide-dominated mountain belt: Central Range, Taiwan, *J. Geol.*, *108*, 73–89.

Howard, A. D. (1997), Badland morphology and evolution: Interpretation using a simulation model, *Earth Surf. Processes Landforms*, *22*, 211–227.

Howard, A. D., W. E. Dietrich, and M. A. Seidl (1994), Modeling fluvial erosion on regional to continental scales, *J. Geophys. Res.*, *99*, 13,971–13,986.

Hsieh, M.-L., and P. L. K. Knuepfer (2002), Synchroneity and morphology of Holocene river terraces in the southern Western Foothills, Taiwan: A guide to interpreting and correlating erosional river terraces across growing anticlines, in *Geology and Geophysics of an Arc-Continent Collision, Taiwan*, edited by T. B. Byrne and C. S. Liu, *Geol. Soc. Am. Spec. Pap.*, *358*, 54–74.

Hsieh, M.-L., P.-M. Liew, and M.-Y. Hsu (2004), Holocene tectonic uplift on the Huatung coast, eastern Taiwan, *Quat. Int.*, *115–116*, 47–70, doi:10.1016/S1040-6182(03)00096-X.

Ijjasz-Vasquez, E. J., and R. L. Bras (1995), Scaling regimes of local slope versus contributing area in digital elevation models, *Geomorphology*, *12*, 299–311.

Iverson, R. M., and J. W. Vallance (2001), New views of granular mass flows, *Geology*, *29*, 115–118.

Kirby, E., and K. Whipple (2001), Quantifying differential rock-uplift rates via stream profile analysis, *Geology*, *29*, 415–418.

Kobor, J. S., and J. J. Roering (2004), Systematic variation of bedrock channel gradients in the central Oregon Coast Range: Implications for rock uplift and shallow landsliding, *Geomorphology*, *62*, 239–256.

Komar, P. D. (1977), Computer simulation of turbidity current flow and the study of deep-sea channels and fan sedimentation, in *The Sea*, vol. 6, *Marine Modelling*, edited by E. D. Goldberg, I. N. McCave, and J. J. O'Brien, chap. 15, pp. 603–621, Wiley-Interscience, Hoboken, N. J.

Kostic, S., G. Parker, and J. Marr (2002), Role of turbidity currents in setting the foreset slope of clinoforms prograding into standing fresh water, *J. Sediment. Res.*, *72*, 353–362.

Kuenen, P. H. (1937), Experiments in connection with Daly's hypothesis on the formation of submarine canyons, *Leidse Geol. Meded.*, *8*, 327–351.

Lague, D., and P. Davy (2003), Constraints on the long-term colluvial erosion law by analyzing slope-area relationships at various tectonic uplift rates in the Siwaliks Hills (Nepal), *J. Geophys. Res.*, *108*(B2), 2129, doi:10.1029/2002JB001893.

Lague, D., P. Davy, and A. Crave (2000), Estimating uplift rate and erodibility from the area-slope relationship: Examples from Brittany and numerical modelling, *Phys. Chem. Earth*, *25*, 543–548.

Lague, D., A. Crave, and P. Davy (2003), Laboratory experiments simulating the geomorphic response to tectonic uplift, *J. Geophys. Res.*, *108*(B1), 2008, doi:10.1029/2002JB001785.

Lavé, J., and J. P. Avouac (2001), Fluvial incision and tectonic uplift across the Himalayas of central Nepal, *J. Geophys. Res.*, *106*, 26,561–26,591.

Li, Y.-H. (1976), Denudation of Taiwan island since the Pliocene epoch, *Geology*, *4*, 105–107.

Lin, A. T., A. B. Watts, and S. P. Hesselbo (2003), Cenozoic stratigraphy and subsidence history of the South China Sea margin in the Taiwan region, *Basin Res.*, *15*, 453–478.

Malavieille, J., et al. (2002), Arc-continent collision in Taiwan: New marine observations and tectonic evolution, in *Geology and Geophysics of an Arc-Continent Collision, Taiwan*, edited by T. B. Byrne and C. S. Liu, *Geol. Soc. Am. Spec. Pap.*, *358*, 189–213.

Marr, J. G., P. A. Harff, G. Shanmugam, and G. Parker (2001), Experiments on subaqueous sandy gravity flows: The role of clay and water content in flow dynamics and depositional structures, *Geol. Soc. Am. Bull.*, *113*, 1377–1386.

Middleton, G. V. (1966a), Experiments on density and turbidity currents: 1. Motion of the head, *Can. J. Earth Sci.*, *3*, 523–546.

Middleton, G. V. (1966b), Experiments on density and turbidity currents: 2. Uniform flow of density currents, *Can. J. Earth Sci.*, *3*, 627–637.

Middleton, G. V., and M. A. Hampton (1973), Sediment gravity flows: Mechanics of flow and deposition, in *Turbidites and Deep-Water Sedimentation*, edited by G. V. Middleton and A. H. Bouma, pp. 1–38, Pac. Sec. Soc. of Econ. Palaeontol. and Mineral., Los Angeles, Calif.

Middleton, G. V., and J. B. Southard (1984), *Mechanics of Sediment Movement*, *Short Course Notes*, vol. 3, 2nd ed., Soc. of Econ. Palaeontol. and Mineral., Los Angeles, Calif.

Mitchell, N. (2004), Form of submarine erosion from confluences in Atlantic USA continental slope canyons, *Am. J. Sci.*, *304*, 590–611.

Mitchell, N. (2005), Interpreting long-profiles of canyons in the USA Atlantic continental slope, *Mar. Geol.*, *214*, 75–99.

Mohrig, D., K. X. Whipple, M. Hondzo, C. Ellis, and G. Parker (1998), Hydroplaning of subaqueous debris flows, *GSA Bull.*, *110*(3), 387–394.

Mohrig, D., A. Elverhøi, and G. Parker (1999), Experiments on the relative mobility of muddy subaqueous and subaerial debris flows, and their capcity to remobilize antecedent deposits, *Mar. Geol.*, *154*, 117–129.

Montgomery, D. R., and W. E. Dietrich (1994), A physically based model for the topographic control on shallow landsliding, *Water Resour. Res.*, *30*, 1153–1171.

Montgomery, D. R., and E. Foufoula-Georgiou (1993), Channel network source representation using digital elevation models, *Water Resour. Res.*, *29*, 3925–3934.

Montgomery, D. R., G. Balco, and S. D. Willett (2001), Climate, tectonics, and the morphology of the Andes, *Geology*, *29*, 579–582.

Mulder, T., B. Savoye, and J. P. M. Syvitski (1997), Numerical modelling of a mid-sized gravity flow: The 1979 Nice turbidity current, *Sedimentology*, *44*, 305–326.

Mulder, T., J. Syvitski, and K. Skene (1998), Modeling of erosion and deposition by turbidity currents generated at river mouths, *J. Sediment. Res.*, *68*, 124–137.

O'Grady, D. B., J. P. M. Syvitski, L. F. Pratson, and J. F. Sarg (2000), Categorizing the morphologic variability of siliciclastic passive continental margins, *Geology*, *28*, 207–210.

Orange, D. L., R. S. Anderson, and N. A. Breen (1994), Regular canyon spacing in the submarine environment: The link between hydrology and geomorphology, *GSA Today*, *4*(2), 29, 36–39.

Parker, G., Y. Fukushima, and H. M. Pantin (1986), Self-accelerating turbidity currents, *J. Fluid Mech.*, *171*, 145–181.

Peakall, J., B. McCaffrey, and B. Kneller (2000), A process model for the evolution, morphology, and architecture of sinuous submarine channels, *J. Sediment. Res.*, *70*, 434–448.

Pratson, L. F., and B. J. Coakley (1996), A model for the headward erosion of submarine canyons induced by downslope-eroding sediment flows, *GSA Bull.*, *108*(2), 225–234.

Pratson, L. F., and W. F. Haxby (1996), What is the slope of the U.S. continental slope?, *Geology*, *24*, 3–6.

Pratson, L. F., W. B. F. Ryan, G. S. Mountain, and D. C. Twichell (1994), Submarine canyon initiation by downslope-eroding sediment flows: Evidence in late Cenozoic strata on the New Jersey continental slope, *GSA Bull.*, *106*(3), 395–412.

Saffer, D. M., and B. A. Bekins (2002), Hydrologic controls on the morphology and mechanics of accretionary wedges, *Geology*, *30*, 271–274.

Schlager, W., and E. W. Adams (2001), Model for the sigmoidal curvature of submarine slopes, *Geology*, *29*, 883–886.

Schmidt, K. M., and D. R. Montgomery (1995), Limits to relief, *Science*, *270*, 617–620.

Schorghofer, N., and D. H. Rothman (2001), Basins of attraction on random topography, *Phys. Rev. E*, *63*, 026112.

Schorghofer, N., and D. H. Rothman (2002) Acausal relations between topographic slope and drainage area, *Geophys. Res. Lett.*, *29*(13), 1633, doi:10.1029/2002GL015144.

Seeber, L., and V. Gornitz (1983), River profiles along the Himalayan arc as indicators of active tectonics, *Tectonophysics*, *92*, 335–367.

Seidl, M. A., and W. E. Dietrich (1992), The problem of channel erosion into bedrock, *Catena Suppl.*, *23*, 101–124.

Selby, M. J. (1993), *Hillslope Materials and Processes*, Oxford Univ. Press, New York.

Shepard, F. P. (1981), Submarine canyons: Multiple causes and long-time persistence, *AAPG Bull.*, *65*(6), 1062–1077.

Shyu, J. B. H., K. Sieh, and Y.-G. Chen (2005), Tandem suturing and disarticulation of the Taiwan orogen revealed by its neotectonic elements, *Earth Planet. Sci. Lett.*, *233*, 167–177.

Sklar, L., and W. E. Dietrich (1998), River longitudinal profiles and bedrock incision models: Stream power and the influence of sediment supply, in *Rivers Over Rock: Fluvial Processes in Bedrock Channels*, *Geophys. Monogr. Ser.*, vol. 107, edited by K. J. Tinkler and E. E. Wohl, pp. 237–260, AGU, Washington, D. C.

Snyder, N. P., K. X. Whipple, G. E. Tucker, and D. J. Merritts (2000), Landscape response to tectonic forcing: Digital elevation model analysis of stream profiles in the Mendocino triple junction region, northern California, *Geol. Soc. Am. Bull.*, *112*, 1250–1263.

Spinelli, G. A., and M. E. Field (2001), Evolution of continental gullies on the northern California margin, *J. Sediment. Res.*, *71*, 237–245.

Stark, C. P., and G. J. Stark (2001), A channelization model of landscape evolution, *Am. J. Sci.*, *301*, 486–512.

Stock, J., and W. E. Dietrich (2003), Valley incision by debris flows: Evidence of a topographic signature, *Water Resour. Res.*, *39*(4), 1089, doi:10.1029/2001WR001057.

Suppe, J. (1980), Imbricated structure of Western Foothills belt, southcentral Taiwan, *Petrol. Geol. Taiwan*, *17*, 1–16.

Suppe, J. (1981), Mechanics of mountain building and metamorphism in Taiwan, *Mem. Geol. Soc. China*, *4*, 67–89.

Tarboton, D. G. (1997), A new method for the determination of flow direction and contributing areas in grid digital elevation models, *Water Resour. Res.*, *33*, 309–319.

Tarboton, D. G., R. L. Bras, and I. Rodriguez-Iturbe (1989), Scaling and elevation in river networks, *Water Resour. Res.*, *25*, 2037–2051.

Teng, L. S. (1990), Geotectonic evolution of Late Cenozoic arc continent collision in Taiwan, *Tectonophysics*, *183*, 57–76.

Teng, L. S., C. T. Lee, Y. B. Tsai, and L.-Y. Hsiao (2000), Slab breakoff as a mechanism for flipping of subduction polarity in Taiwan, *Geology*, *28*, 155–158.

Tucker, G. E., and R. L. Bras (1998), Hillslope processes, drainage density, and landscape morphology, *Water Resour. Res.*, *34*, 2751–2764.

Tucker, G. E., and K. X. Whipple (2002), Topographic outcomes predicted by stream erosion models: Sensitivity analysis and intermodel comparison, *J. Geophys. Res.*, *107*(B9), 2179, doi:10.1029/2001JB000162.

Twichell, D. C., and D. G. Roberts (1982), Morphology, distribution, and development of submarine canyons on the United States Atlantic continental slope between Hudson and Baltimore canyons, *Geology*, *10*, 408–412.

Whipple, K. X. (2000), Rates and processes of bedrock incision by the Upper Ukak River since the 1912 Novarupta ash flow in the Valley of Ten Thousand Smokes, Alaska, *Geology*, *28*, 835–838.

Whipple, K. X. (2004), Bedrock rivers and the geomorphology of active orogens, *Annu Rev. Earth Planet. Sci.*, *32*, 151–185.

Whipple, K. X., and B. J. Meade (2004), Controls on the strength of coupling among climate, erosion, and deformation in two-sided, frictional orogenic wedges at steady state, *J. Geophys. Res.*, *109*, F01011, doi:10.1029/2003JF000019.

Whipple, K. X., and G. E. Tucker (1999), Dynamics of the stream-power river incision model: Implications for height limits of mountain ranges, landscape response timescales, and research needs, *J. Geophys. Res.*, *104*(B8), 17,661–17,674.

Whipple, K. X., and G. E. Tucker (2002), Implications of sediment-flux-dependent river incision models for landscape evolution, *J. Geophys. Res.*, *107*(B2), 2039, doi:10.1029/2000JB000044.

Willett, S. D., and M. T. Brandon (2002), On steady states in mountain belts, *Geology*, *30*, 175–178.

Willett, S. D., C. Beaumont, and P. Fullsack (1993), Mechanical model for the tectonics of doubly vergent compressional orogens, *Geology*, *21*, 371–374.

Willett, S. D., R. Slingerland, and N. Hovius (2001), Uplift, shortening, and steady state topography in active mountain belts, *Am. J. Sci.*, *301*, 455–485.

Willett, S. D., D. Fisher, C. Fuller, E. C. Yeh, and C. Y. Lu (2003), Erosion rates and orogenic wedge kinematics in Taiwan inferred from apatite fission track thermochronometry, *Geology*, *31*, 945–948.

Willgoose, G. (1994), A physical explanation for an observed area-slope-elevation relationship for catchments with declining relief, *Water Resour. Res.*, *30*, 151–159.

Willgoose, G., R. L. Bras, and I. Rodriguez-Iturbe (1991), Results from a new model of river basin evolution, *Earth Surf. Processes Landforms*, *16*, 237–254.

Wobus, C. W., K. V. Hodges, and K. X. Whipple (2003), Has focused denudation sustained active thrusting at the Himalayan topographic front?, *Geology*, *31*, 861–864.

Yu, S.-B., H.-Y. Chen, and L.-C. Kuo (1997), Velocity field of GPS stations in the Taiwan area, *Tectonophysics*, *274*, 41–59.

N. Hovius, Department of Earth Sciences, University of Cambridge, Downing Street, Cambridge CB2 3EQ, UK.

D. Lague, UMR 6118, Géosciences Rennes, CNRS, Campus de Beaulieu, F-35042 Rennes Cedex, France.

C.-S. Liu, Oceanography, National Taiwan University, No. 1, Sec. 4, Roosevelt Road, Taipei 10617, Taiwan.

L. A. Ramsey, Bullard Laboratories, Department of Earth Sciences, University of Cambridge, Madingley Road, Cambridge CB3 0EZ, UK. (lar26@esc.cam.ac.uk)